Supplementary Information for

Orthogonally photogated electron transport through π-π supramolecular junctions of donor-acceptor Stenhouse adducts

Gaolu Zhu[1#], Hanjun Zhang[1, 2#], Yangyang Pan[1], Xin Zuo[3], Yu Zhou[4*], Wenshu Liu[1], Hongyang Zhang[1], Tianfang Shi[1], Xinyu Chen[1], Huanqi Qin[1], Chen Wei[1], Xu Deng[5], Lichuan Chen[3], Fanxi Sun[1]*, Yonghao Zheng[1]*, Dongsheng Wang[1]*

[1]School of Optoelectronic Science and Engineering, University of Electronic Science and Technology of China, Chengdu 610054, China.

[2]School of Pharmacy, Qujing University of Medicine & Health Sciences, Qujing 655100, China.

[3]Institute of Modern Optics, Center of Single-Molecule Sciences, Tianjin Key Laboratory of Micro-Scale Optical Information Science and Technology, Nankai University, Tianjin 300350, China.

[4]College of Chemistry, Huazhong Agricultural University, Wuhan, 430070, China.

[5]Institute of Fundamental and Frontier Sciences, University of Electronic Science and Technology of China, Chengdu 610054, China.

[#]These authors contributed equally:

Corresponding Authors: Yu Zhou (yuzhou@mail.hzau.edu.cn), Fanxi Sun (fanxi_sun@uestc.edu.cn), Yonghao Zheng (zhengyonghao@uestc.edu.cn) and Dongsheng Wang (wangds@uestc.edu.cn).

Table of Contents

1. Synthesis and molecular characterization

Compounds **1**, **5** and **6** were prepared according to previously reported procedures[1, 2, 3]. The synthetic routes to D1, D2 and D3 are shown in Supplementary Figs. 1-4. Unless otherwise stated, all reactions were performed under ambient atmosphere using commercially available solvents and reagents.

Synthesis of **D1**:

Supplementary Fig. 1 | Synthesis of D1

Compound **1** (278 mg, 1.00 mmol) was dissolved in DCM (4 mL) and hexafluoroisopropanol (HFIP, 0.5 mL) was added, followed by the slow addition of indoline (compound 2, 0.15 g, 1.26 mmol). The reaction mixture was stirred at room temperature for 1 h. Then, diethyl ether (30 mL) was slowly added to the reaction mixture, and the mixture was gently stirred for 5 min. The resulting solid was collected by filtration and washed several times with diethyl ether to afford **D1** as a dark green powder (286 mg, 72%).

^{1}H NMR (600 MHz, $C_2D_2Cl_4$) δ (ppm): 12.70 (s, 1H), 7.82 (d, 1H), 7.22 (s, 1H), 7.21 – 7.18 (m, 2H), 7.15 (d, *J* = 6.6 Hz, 1H), 6.88 (d, *J* = 12.7 Hz, 1H), 6.78 (t, *J* = 15.1, 1H), 6.30 (t, *J* = 12.6, 1H), 4.55 (dq, *J* = 21.9, 6.9 Hz, 4H), 3.58 (t, *J* = 8.4 Hz, 2H), 3.05 (t, *J* = 8.3 Hz, 2H), 1.33 – 1.27 (m, 6H)

^{13}C NMR (151 MHz, $CDCl_3$) δ (ppm): 177.44, 163.04, 157.65, 149.37, 147.21, 143.47, 141.03, 132.86, 128.61, 126.07, 110.22, 106.13, 103.31, 70.84, 43.99, 43.16, 29.84, 29.11, 28.39, 27.62, 11.93.

HRMS (ESI$^+$): *m*/*z* found 398.1527 ([**M** + **H**]$^+$); calcd for $C_{21}H_{23}N_3O_3S$ ([**M**]$^+$) 397.1460.

Synthesis of 5-(methylthio)indoline (**4**):

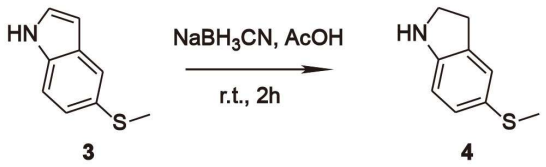

Supplementary Fig. 2 | Synthesis of 4

Reaction was conducted based on the general procedure for reduction of indole. To a solution of 5-(methylthio)-1H-indole (**3**) (500 mg, 3.07 mmol) in AcOH (10 mL) was added $NaBH_3CN$ (316 mg, 5.03 mmol) portionwise over 30 minutes at 0 °C. The resulting mixture was allowed to warm up to room temperature. purified by column chromatography, obtaining 0.48 g orange-yellow product **4** as a yellow oil (Yield: 95%).

^{1}H NMR (400 MHz, CD_2Cl_2) δ (ppm): 7.17 (s, 1H), 7.07 (d, *J* = 8.1 Hz, 1H), 6.58 (d, *J* = 8.1 Hz, 1H), 3.58 (s, 1H), 3.57-3.50 (m, 2H), 3.02 (t, *J* = 8.4 Hz, 2H), 2.43 (s, 3H).

^{13}C NMR (101 MHz, $CDCl_3$) δ (ppm): 155.00, 125.70, 125.05, 122.05, 113.80, 101.12, 52.55, 46.67, 27.59.

Synthesis of **D2**:

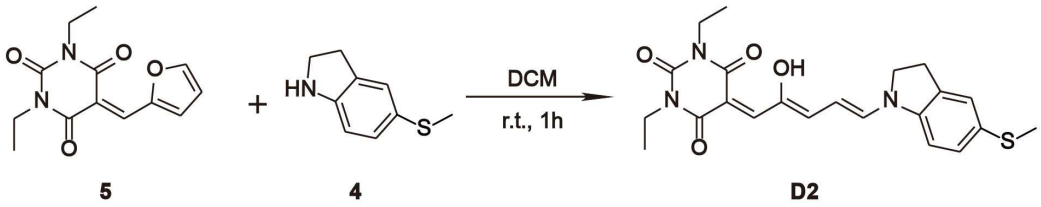

Supplementary Fig. 3 | Synthesis of D2

Compound **5** (0.26 g, 1.00 mmol) and compound **4** (0.20 g, 1.21 mmol) were sequentially added to DCM (4 mL), and HFIP (0.5 mL) was added. The reaction mixture was stirred at room temperature for 1 h. Then, diethyl ether (30 mL) was slowly added to the reaction mixture, and the mixture was gently stirred for 5 min. The resulting solid was collected by filtration and washed several times with diethyl ether to afford **D2** as a dark blue powder (260 mg, 61%).

^{1}H NMR (600 MHz, $C_2D_2Cl_4$) δ (ppm): 12.55 (s, 1H), 7.62 (d, *J* = 12.6 Hz, 1H), 7.30 (s, 1H), 7.16 (dd, *J* = 10.7 Hz, 2H), 7.04 (d, *J* = 9.2 Hz, 1H), 6.70 (d, *J* = 12.2 Hz, 1H), 6.14 (t, *J* = 12.5 Hz, 1H), 4.11 (t, *J* = 8.2 Hz, 2H), 3.99 – 3.94 (m, 4H), 3.28 (t, *J* = 8.2 Hz, 2H), 2.49 (s, 3H), 1.21 (t, *J* = 7.8 Hz, 6H).

^{13}C NMR (151 MHz, $CDCl_3$) δ (ppm): 171.99, 167.43, 166.51, 150.32, 132.46, 129.56, 114.47, 71.89, 70.48, 69.79, 64.72, 62.19, 47.55, 45.93, 37.65, 34.99, 31.64, 28.24, 26.94, 18.87, 14.13, 12.05.

HRMS (ESI^{+}): *m/z* found 427.1556 [**M**]$^{+}$, 428.1627 ([**M** + **H**]$^{+}$); calcd for $C_{22}H_{25}N_3O_4S$ [**M**]$^{+}$ 427.1566, ([**M** + **H**]$^{+}$) 428.1639.

Synthesis of **D3**:

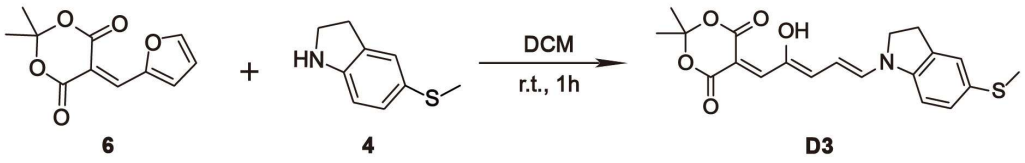

Supplementary Fig. 4 | Synthesis of D3

Compound **6** (0.222 g, 1 mmol) and 5-(methylthio)indoline (compound **4**, 0.2 g, 1.21 mmol) were added sequentially to 4 mL of DCM, and HFIP (0.5 mL) was added. After stirring at room temperature for 1 h, then 30 mL diethyl ether was slowly poured into the beaker, and slowly stirred for 5 min. The obtained solid was filtered and washed with diethyl ether several times to obtain dark blue **D3** powder (182 mg, 47%).

^{1}H NMR (600 MHz, CD_2Cl_2) δ (ppm): 11.34 (s, 1H), 7.62 (d, *J* = 12.5 Hz, 1H), 7.32 (s, 1H), 7.18 (dd, *J* = 7.5 Hz, 2H), 7.02 (d, *J* = 8.4 Hz, 1H), 6.67 (d, *J* = 11.6 Hz, 1H), 6.16 (d, *J* = 12.3 Hz, 1H), 4.10 (t, *J* = 8.2 Hz, 2H), 3.29 (t, *J* = 8.1 Hz, 2H), 2.49 (s, 3H), 1.73 (s, 6H).

^{13}C NMR (151 MHz, $CDCl_3$) δ (ppm): 164.74, 145.06, 144.02, 141.93, 140.44, 136.14, 133.32, 127.36, 121.80, 120.69, 105.95, 102.17, 47.93, 46.37, 44.65, 29.85, 28.22, 27.50, 26.61, 17.42.

HRMS (ESI$^+$): *m/z* found 387.1112 [**M**]$^+$, 388.1195 ([**M** + **H**]$^+$); calcd for $C_{20}H_{21}NO_5S$ [**M**]$^+$ 387.1140, ([**M** + **H**]$^+$) 388.1214.

2. Single-crystal structures of DASAs

Single crystals of D1, D2, and D3 were obtained via a low-temperature solvent evaporation method. Initially, an excess of the DASAs was fully dissolved in dichloromethane (DCM) or tetrahydrofuran (THF) at 30 °C to ensure the formation of a saturated solution. The mixture was then filtered through a Teflon membrane into a 20 mL glass vial. To induce crystallization, the solvent was allowed to evaporate slowly at a controlled temperature of 4 °C. The resulting crystals were subsequently collected for further structural analysis. Crystal structure data of D1, D2, and D3 are shown in Supplementary Figs. 5-S7. Single-crystal structure analysis clarifies the distinct π-π stacking geometries of D1, D2, and D3 in the solid state, where the plane-to-plane distances of their respective dimers are consistently maintained within the range of 3~4 Å.

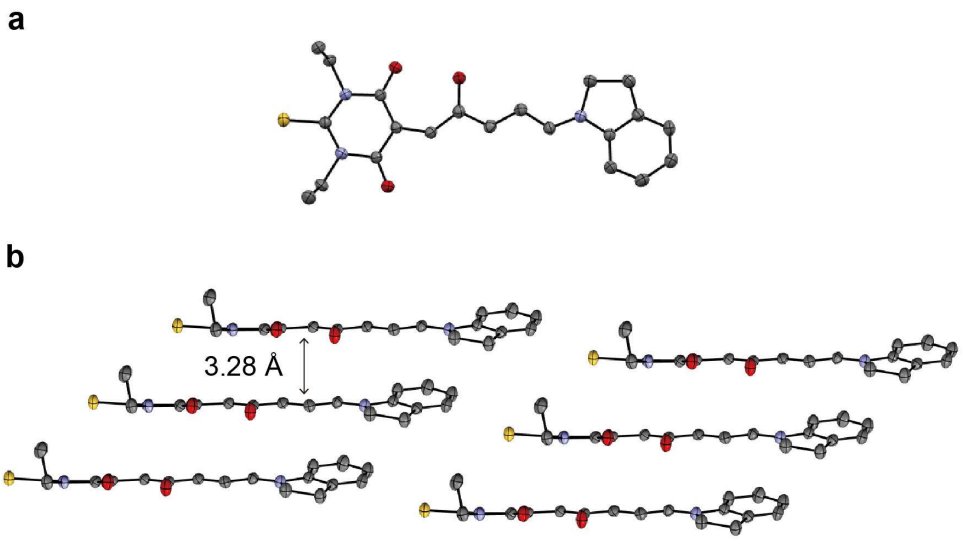

Supplementary Fig. 5 | Single-crystal structure and packing of D1. a, Single-crystal structure of D1. Hydrogen atoms are omitted for clarity. **b,** Crystal packing of D1 showing π-π stacking between neighboring molecules with an intermolecular distance of 3.28 Å. Crystallographic data are available from the Cambridge Crystallographic Data Centre via www.ccdc.cam.ac.uk/data_request/cif CCDC# 2536483.

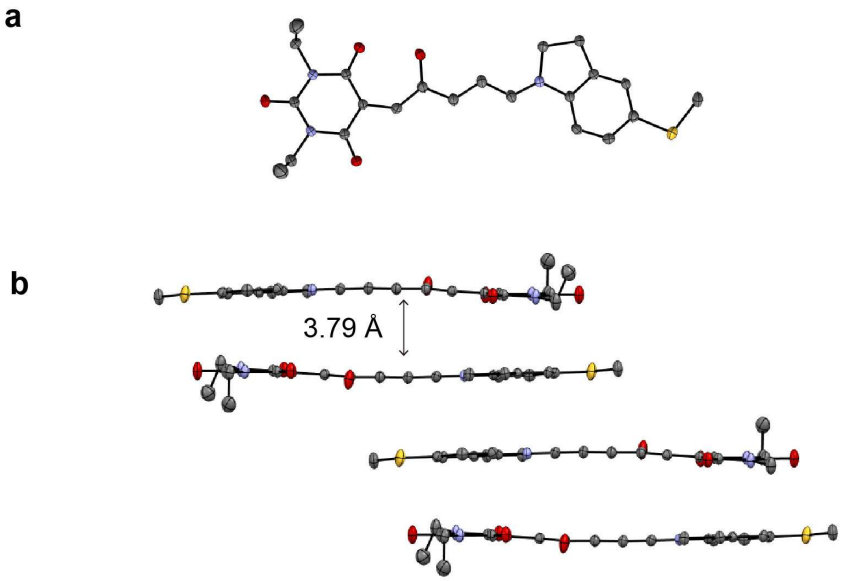

Supplementary Fig. 6 | Single-crystal structure and packing of D2. a, Single-crystal structure of D2. Hydrogen atoms are omitted for clarity. **b,** Crystal packing of D2 showing the π-stacked arrangement between neighboring molecules with an intermolecular distance of 3.79 Å. Crystallographic data are available from the Cambridge Crystallographic Data Centre via www.ccdc.cam.ac.uk/data_request/cif CCDC# 2536489.

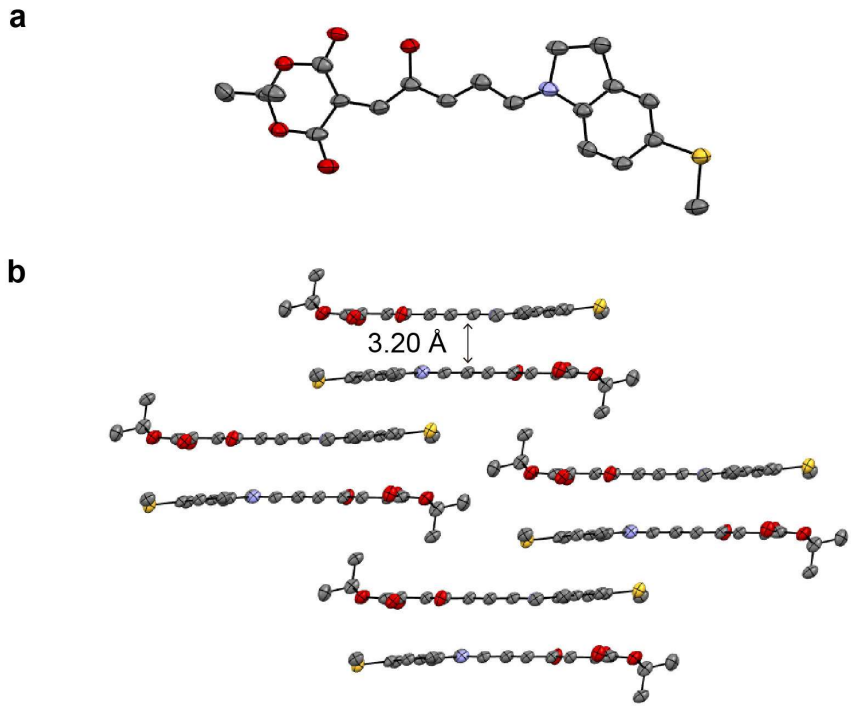

Supplementary Fig. 7 | Single-crystal structure and packing of D3. a, Single-crystal structure of D3. Hydrogen atoms are omitted for clarity. **b,** Crystal packing of D3 showing the π-stacked arrangement between neighboring molecules with an intermolecular distance of 3.20 Å. Crystallographic data are available from the Cambridge Crystallographic Data Centre via www.ccdc.cam.ac.uk/data_request/cif CCDC# 2536490.

3. Optical and photoisomerization properties of DASAs

3.1 Optical property of DASAs

3.1.1 Molar absorption coefficients of D1 and D3 at selected wavelengths

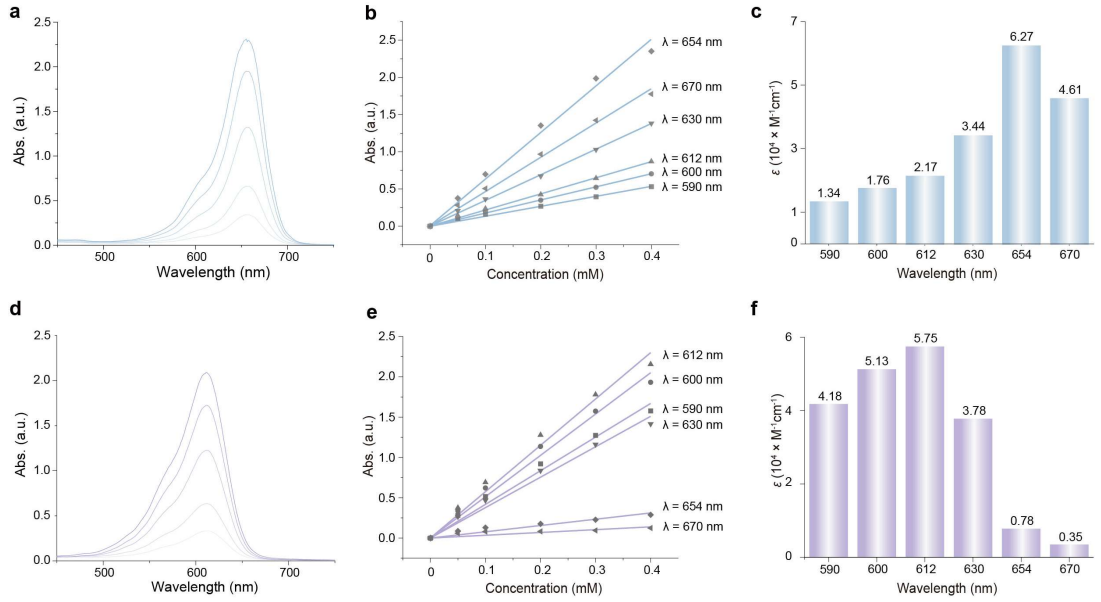

Supplementary Fig. 8 | Molar absorption coefficients of D1 and D3. a, d, Concentration-dependent UV-vis absorption spectra, **b, e**, Absorbance-concentration calibration curves at six representative wavelengths, and **c, f** Calculated molar absorption coefficients of D1 and D3 in TCB, respectively. All spectra were recorded using a 1 mm path-length quartz cuvette. The molar absorption coefficients were calculated using the Beer-Lambert law, $A = \varepsilon cL$, with $L = 0.1$ cm. Values are reported as ε in $10^4 \times M^{-1}cm^{-1}$.

The molar absorption coefficients of D1 and D3 were determined at six selected wavelengths because their absorption spectra overlap. These calibrated ε values provide the basis for the subsequent spectral deconvolution and orthogonality analysis of the D1/D3 mixed system in Section 5.

3.1.2 Molar absorption coefficient of D2 at λ_{max}

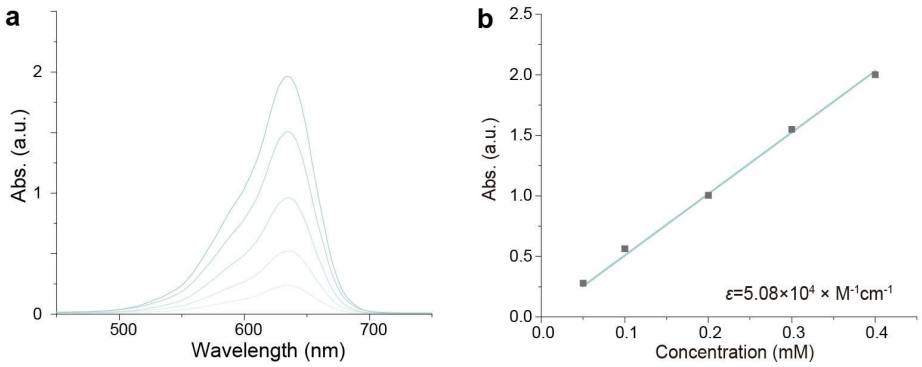

Supplementary Fig. 9 | Molar absorption coefficients of D2. a, Concentration-dependent UV-vis absorption spectra. **b,** Absorbance-concentration calibration curves at λ_{max} (635 nm). The spectra were recorded using a 1 mm path-length quartz cuvette. The molar absorption coefficient was calculated using the Beer-Lambert law, $A = \varepsilon cL$, with L = 0.1 cm.

3.2 Isomerization kinetics

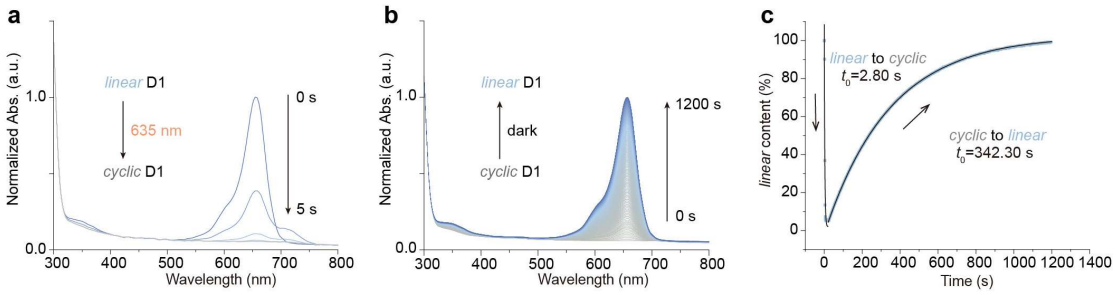

Supplementary Fig. 10 | Photoisomerization and thermal recovery kinetics of D1 in TCB. a, Time-dependent UV-vis absorption spectra of D1 (0.020 mM in TCB) under continuous irradiation at 635 nm (1 mW/cm^2). **b,** Thermal recovery of D1 monitored by UV-vis absorption spectra in the dark at 20 °C after irradiation. **c,** Kinetics of *linear*-to-*cyclic* isomerization under 635 nm irradiation (1 mW/cm^2) and *cyclic*-to-*linear* thermal recovery in the dark at 20 °C.

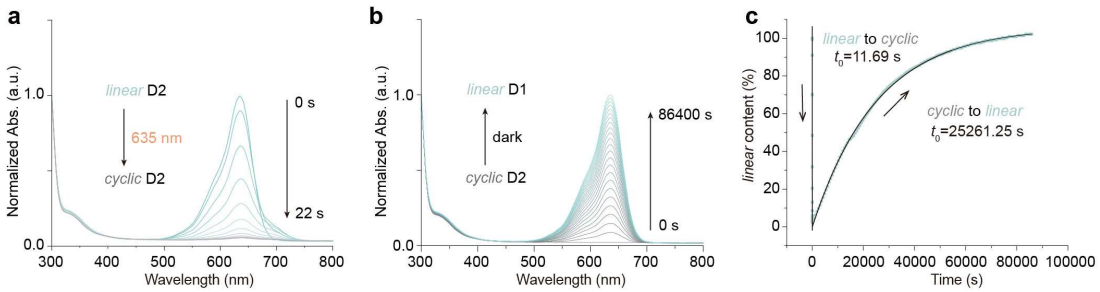

Supplementary Fig. 11 | Photoisomerization and thermal recovery kinetics of D2 in TCB. a, Time-dependent UV-vis absorption spectra of D2 (0.04 mM in TCB) under continuous irradiation at 635 nm (1 mW/cm^2). **b,** Thermal recovery of D2 monitored by UV-vis absorption spectra in the dark at 20 ºC after irradiation. **c,** Kinetics of *linear*-to-*cyclic* isomerization under 635 nm irradiation (1 mW/cm^2) and *cyclic*-to-*linear* thermal recovery in the dark at 20 ºC.

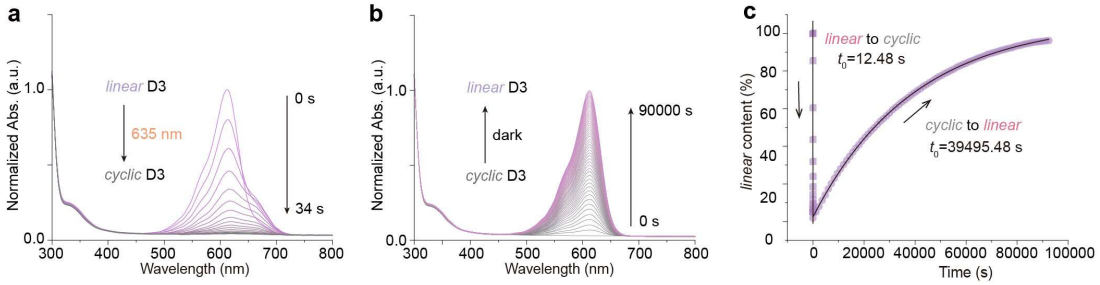

Supplementary Fig. 12 | Photoisomerization and thermal recovery kinetics of D3 in TCB. a, Time-dependent UV-vis absorption spectra of D3 (0.03 mM in TCB) under continuous irradiation at 635 nm (1 mW/cm^2). **a,** Thermal recovery of D3 monitored by UV-vis absorption spectra in the dark at 20 ºC after irradiation. **a,** Kinetics of *linear*-to-*cyclic* isomerization under 635 nm irradiation (1 mW/cm^2) and *cyclic*-to-*linear* thermal recovery in the dark at 20 ºC.

3.3 Reversible photoswitching cycles of DASAs

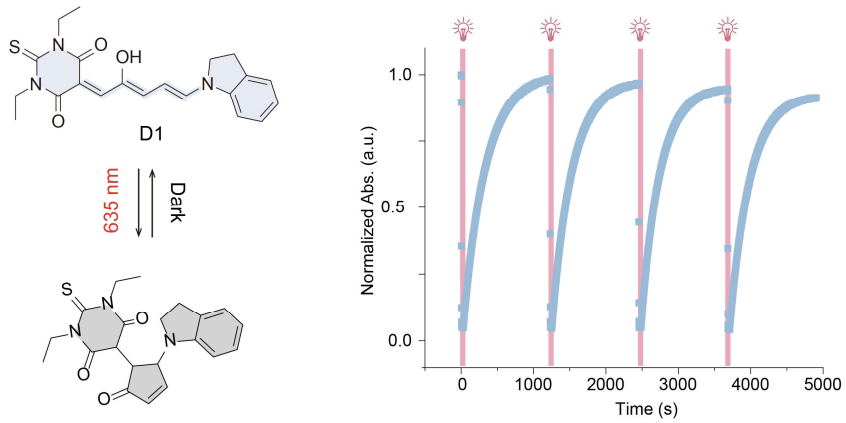

Supplementary Fig. 13 | Reversible photoswitching cycles of D1. Cycling stability of D1 during repeated photoisomerization (635 nm, 1 mW/cm^2) and thermal relaxation (20 °C, dark) in TCB.

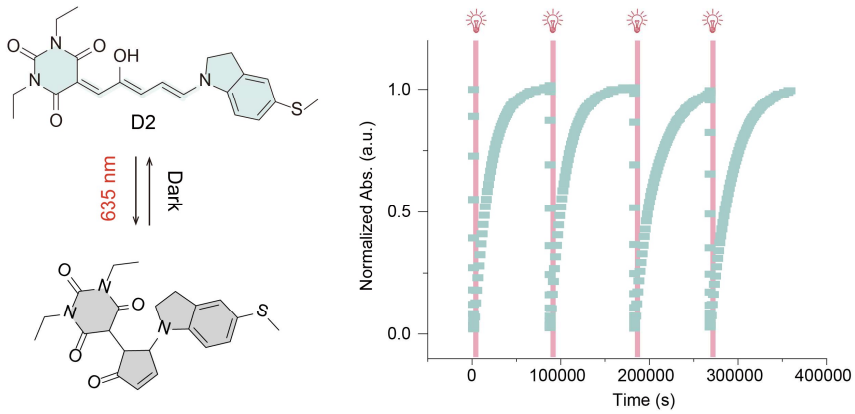

Supplementary Fig. 14 | Reversible photoswitching cycles of D2. Cycling stability of D2 during repeated photoisomerization (635 nm, 1 mW/cm^2) and thermal relaxation (20 °C, dark) in TCB.

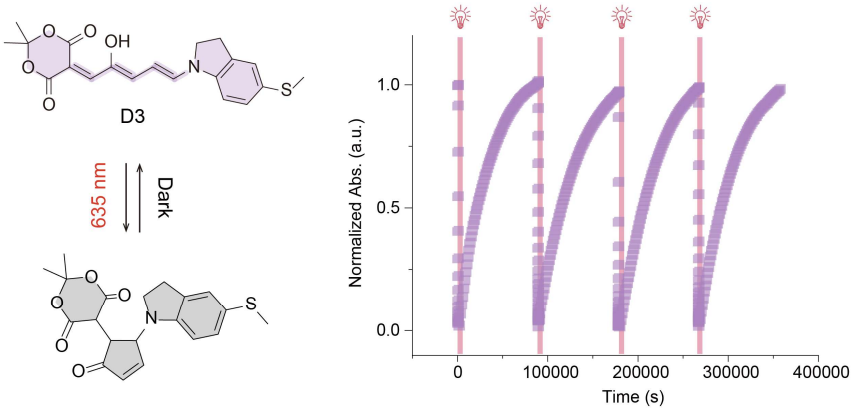

Supplementary Fig. 15 | Reversible photoswitching cycles of D3. Cycling stability of D3 during repeated photoisomerization (635 nm, 1 mW/cm^2) and thermal relaxation (20 °C, dark) in TCB.

3.4 Photoisomerization kinetics of DASAs under light irradiation

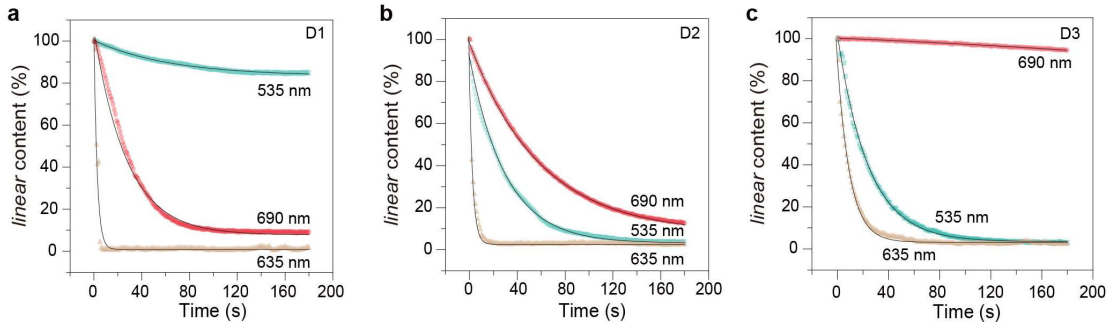

Supplementary Fig. 16 | Photoisomerization kinetics of DASAs under different irradiation wavelengths. Time-dependent evolution of the *linear* content for D1, D2, and D3 (0.03 mM in 1, 2, 4-trichlorobenzene (TCB)) under irradiation at **a,** 535 nm (0.5 mW/cm^2), **b,** 635 nm (1.0 mW/cm^2) and **c,** 690 nm (0.7 mW/cm^2), respectively. The *linear* content is calculated from the normalized intensity of the characteristic absorption band for D1, D2 and D3.

These results indicate a possible wavelength-dependent isomerization kinetics of the DASAs, which were investigated using 535 nm, 635 nm and 690 nm laser as the incident light source. D1 and D3 exhibit clearly wavelength-selective isomerization upon 535 nm and 690 nm irradiation. While 690 nm light (0.7 mW/cm^2) results in a ~92.3% conversion rate at the equilibrium with the rate constant (τ) of 0.036 s^{-1} for D1, the isomerization is largely hindered upon 535 nm light (0.5 mW/cm^2) and the equilibrium conversion rate decreases to ~16.7% (Supplementary Fig. 16a). The isomerization behavior of D3 exhibits an opposite relationship, where 535 nm light induces nearly 100% conversion with the rate constant of 0.041 s^{-1}, only ~6.0% of *cyclic* D3 is formed after 690 nm light irradiation (Supplementary Fig. 13c). Therefore, in the following experiments, while 635 nm light is used to simultaneously trigger the isomerization of all DASAs, D1 and D3 could be orthogonally controlled using the 535 nm and 690 nm irradiation. In contrast, D2 with the absorption spectrum located between D1 and D3 responds efficiently to all these wavelengths (Supplementary Fig. 16b).

4. STM-BJ measurements and computational analysis

4.1 STM-BJ experimental setup and data processing

Single-molecule conductance measurements were performed using a scanning tunneling microscope break-junction (STM-BJ) setup. Gold tips (99.99%, 0.25 mm) were fabricated by melting Au wire into a bead and mounted on a piezoelectric actuator fixed to a stepping motor for coarse control. Gold-coated silicon wafers were used as substrates, cleaned with piranha solution (H_2SO_4/H_2O_2 = 3:1, *v*/*v*), rinsed with ultrapure water (18.25 MΩ·cm) and dried in vacuum prior to each experiment. For each experiment, thousands of conductance traces were collected to analyze 1D conductance histograms and 2D conductance-displacement histograms, facilitating the examination of molecular junction formation. Unless otherwise specified, conductance measurements were performed in the dark at 298 K. During measurements, the gold tip was repeatedly brought into and out of contact with the substrate at 10 nm/s.

Flicker noise analysis was performed to probe the charge transport mechanism[4]. After junction formation, the tip was held for 150 ms and conductance fluctuations were Fourier transformed to obtain power spectral densities (PSDs). Normalized PSD vs. average conductance maps were constructed from thousands of traces, and scaling exponents were extracted using 2D Gaussian fitting. Exponents near 1 indicate through-bond transport, while values near 2 indicate through-space tunneling[4, 5]. The molecular conductance data, including typical individual conductance traces, 1D and 2D conductance-displacement histograms are analyzed with the homemade single-molecule break junctions experimental data processing software built with Python and PyQt5, XMe DataAnalysis, which is available for research users at https://github.com/Pilab-XMU/XMe_DataAnalysis[4].

To resolve transport features from heterogeneous single-molecule conductance datasets, unsupervised K-means clustering was used for trace classification[6, 7]. Conventional 1D and 2D conductance histograms can contain overlapping contributions from different

junction configurations, leading to broadened or partially obscured conductance features. In the conductance-distance analysis, individual traces were grouped according to selected descriptors, including trace shape, plateau length, and conductance distribution. This procedure helps distinguish molecular junction traces from featureless tunneling traces and separates different conductance populations associated with single-molecule and π-π stacked junctions. For *I-V* analysis [6], clustering was further used to separate stable junction *I-V* curves from traces showing large fluctuations or premature junction rupture. The refined datasets were then used for *I-V* fitting and extraction of transport parameters.

4.2 DFT calculation analysis

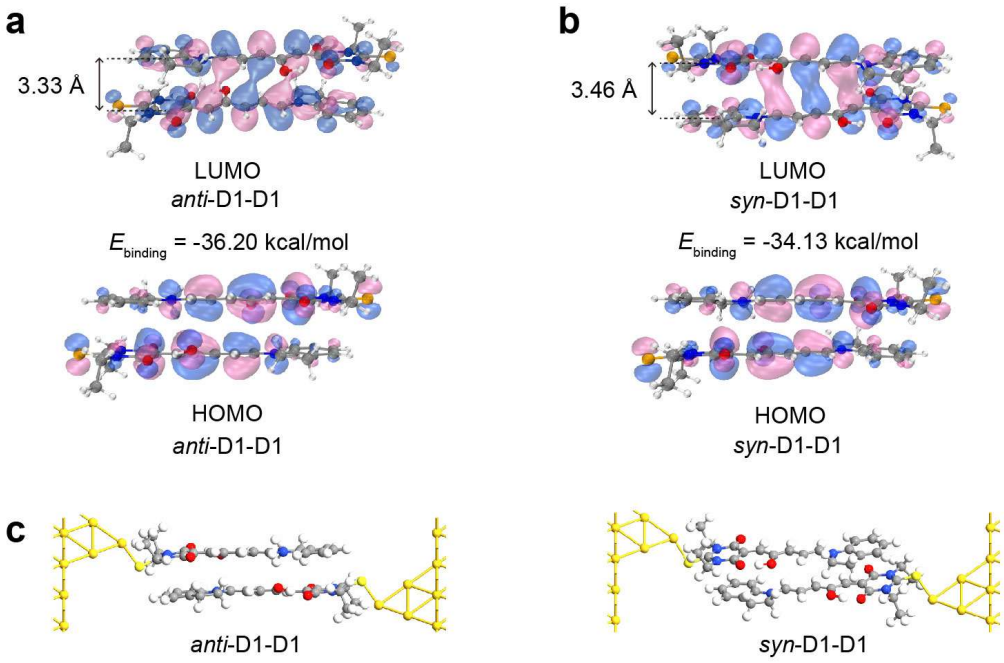

Supplementary Fig. 17 | DFT and transmission analysis of *anti*-D1-D1 and *syn*-D1-D1. LUMO and HOMO distributions of **a,** *Anti*-D1-D1 and **b,** *Syn*-D1-D1, respectively (isovalue = 0.02). **c,** Optimized geometries of the *anti*-D1-D1 and *syn*-D1-D1 π-stacked configurations constructed between Au electrodes.

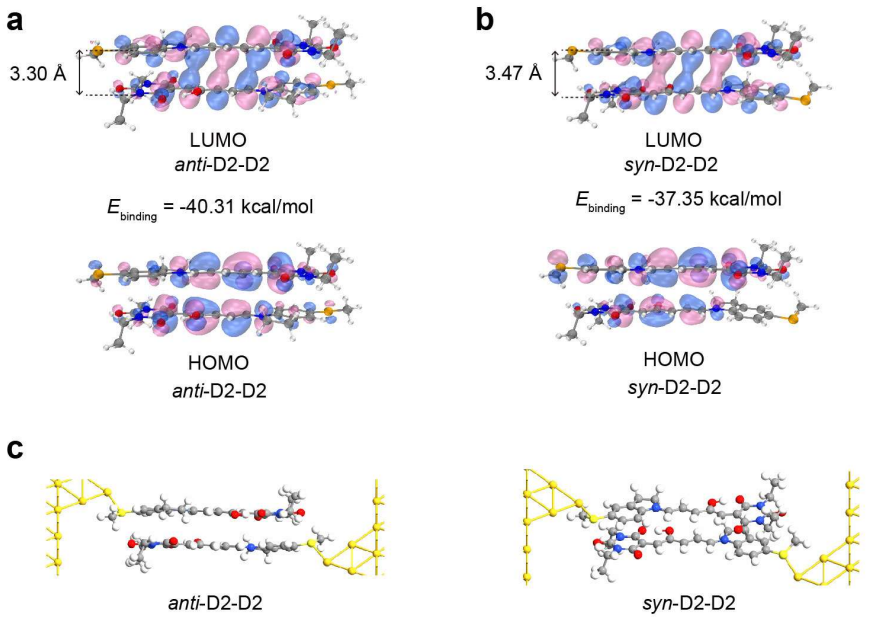

Supplementary Fig. 18 | DFT and transmission analysis of *anti*-D2-D2 and *syn*-D2-D2. LUMO and HOMO distributions of **a,** *Anti*-D1-D1 and **b,** *Syn*-D1-D1, respectively (isovalue = 0.02). **c,** Optimized geometries of the *anti*-D2-D2 and *syn*-D2-D2 π-stacked configurations constructed between Au electrodes.

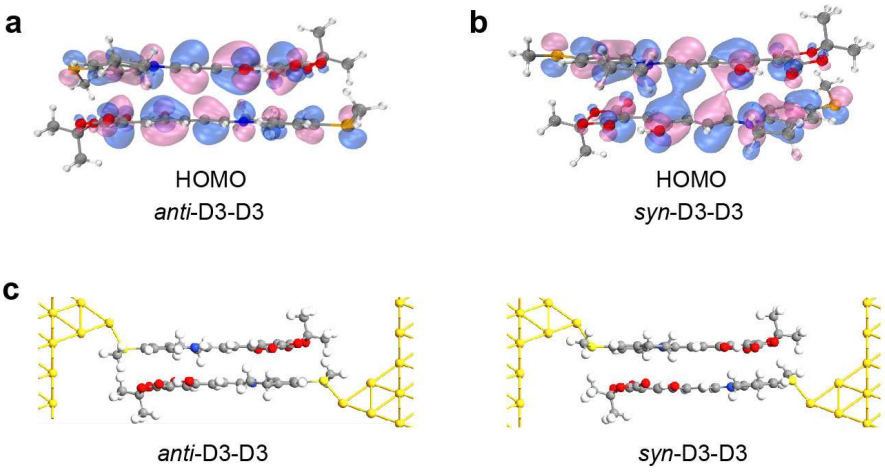

Supplementary Fig. 19 | DFT and transmission analysis of *anti*-D3-D3. HOMO distributions of **a,** *Anti*-D3-D3 and **b,** *Syn*-D3-D3, respectively (isovalue = 0.02). **c,** Optimized geometries of the *anti*-D3-D3 and *syn*-D3-D3 π-stacked configurations constructed between Au electrodes.

In contrast to the LUMO distributions, the HOMO orbitals of both *anti*-D3-D3 and *syn*-D3-D3 are mainly localized on individual D3 molecules and show negligible intermolecular overlap (Supplementary Fig. 19).

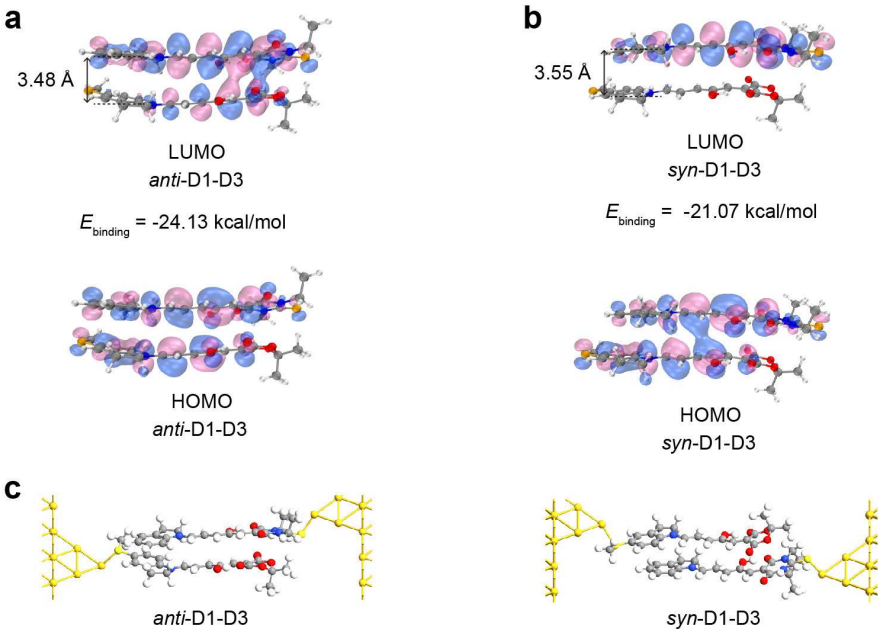

Supplementary Fig. 20 | DFT and transmission analysis of *anti*-D1-D3 and *syn*-D1-D3. LUMO and HOMO distributions of **a,** *Anti*-D1-D1 and **b,** *Syn*-D1-D1, respectively (isovalue = 0.02). **c,** Optimized geometries of the *anti*-D1-D3 and *syn*-D1-D3 π-stacked configurations constructed between Au electrodes.

4.3 Solvent background conductance measurements

Control STM-BJ measurements were performed in pure TCB to evaluate the solvent background. As shown in Supplementary Fig. 21a and S21b, the 1D and 2D conductance histograms of TCB show no distinct conductance peak or molecular plateau feature, indicating that TCB does not contribute significant conductance signals under the present measurement conditions. Therefore, TCB can be used as an inert solvent background for the conductance measurements of the target molecules. The tunneling decay constant (log $(G/G_0)/\Delta z$ = -5.5 nm^{-1}) was used to calibrate the relative displacement distribution in the conductance range from $10^{-3.5}$ G_0 to $10^{-5.5}$ G_0 at 0.36 nm, as shown in the inset of Supplementary Fig. 21c.

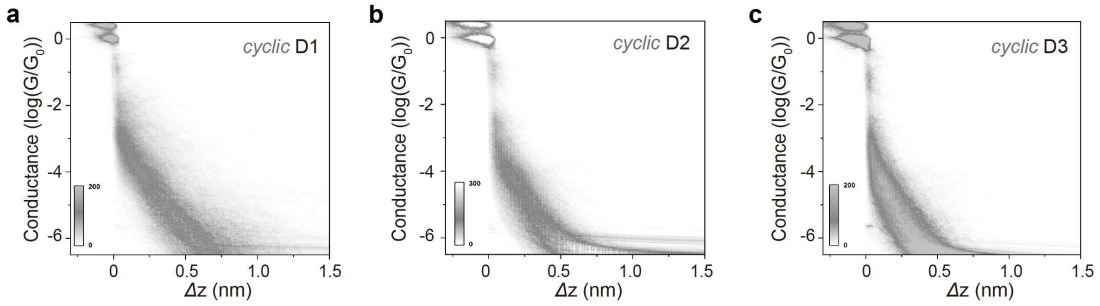

Supplementary Fig. 21 | Solvent background conductance measurements in TCB. **a,** 2D conductance histogram of the TCB at bias voltages of 300 mV. **b,** 1D logarithmic conductance histograms of TCB measured at bias voltages of 300 mV. **c,** 2D conductance versus relative distance (Δz) histogram and the relative displacement distribution histogram determined from the conductance range between $10^{-3.5}$ G_0 to $10^{-5.5}$ G_0.

4.4 Individual conductance traces of DASAs *homo*-junctions

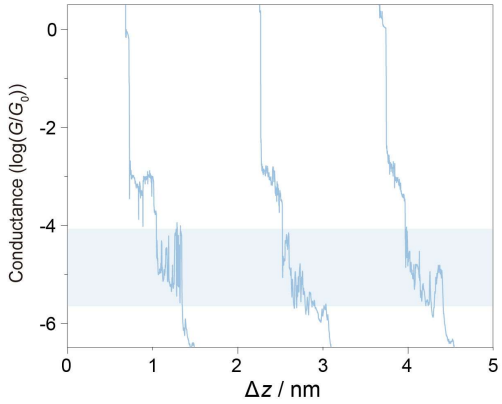

Supplementary Fig. 22 | The typical individual conductance traces for D1 *homo*-junctions.

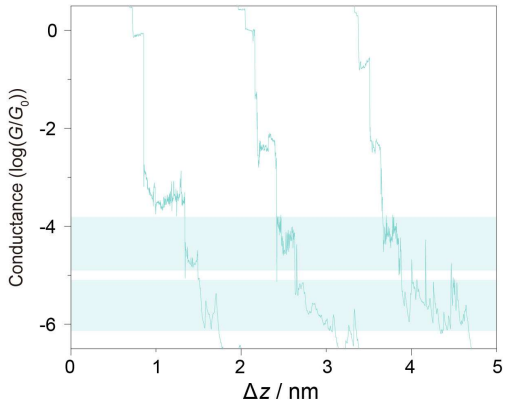

Supplementary Fig. 23 | The typical individual conductance traces for D2 *homo*-junctions.

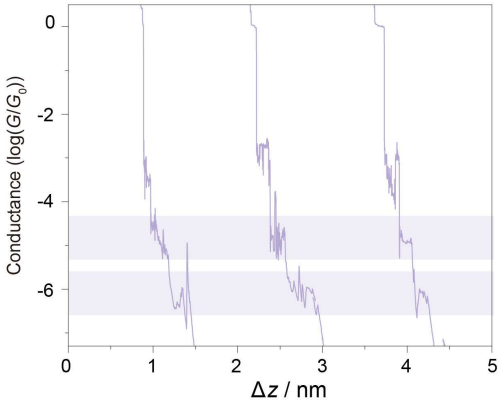

Supplementary Fig. 24 | The typical individual conductance traces for D3 *homo*-junctions.

4.5 Concentration-dependent conductance measurements

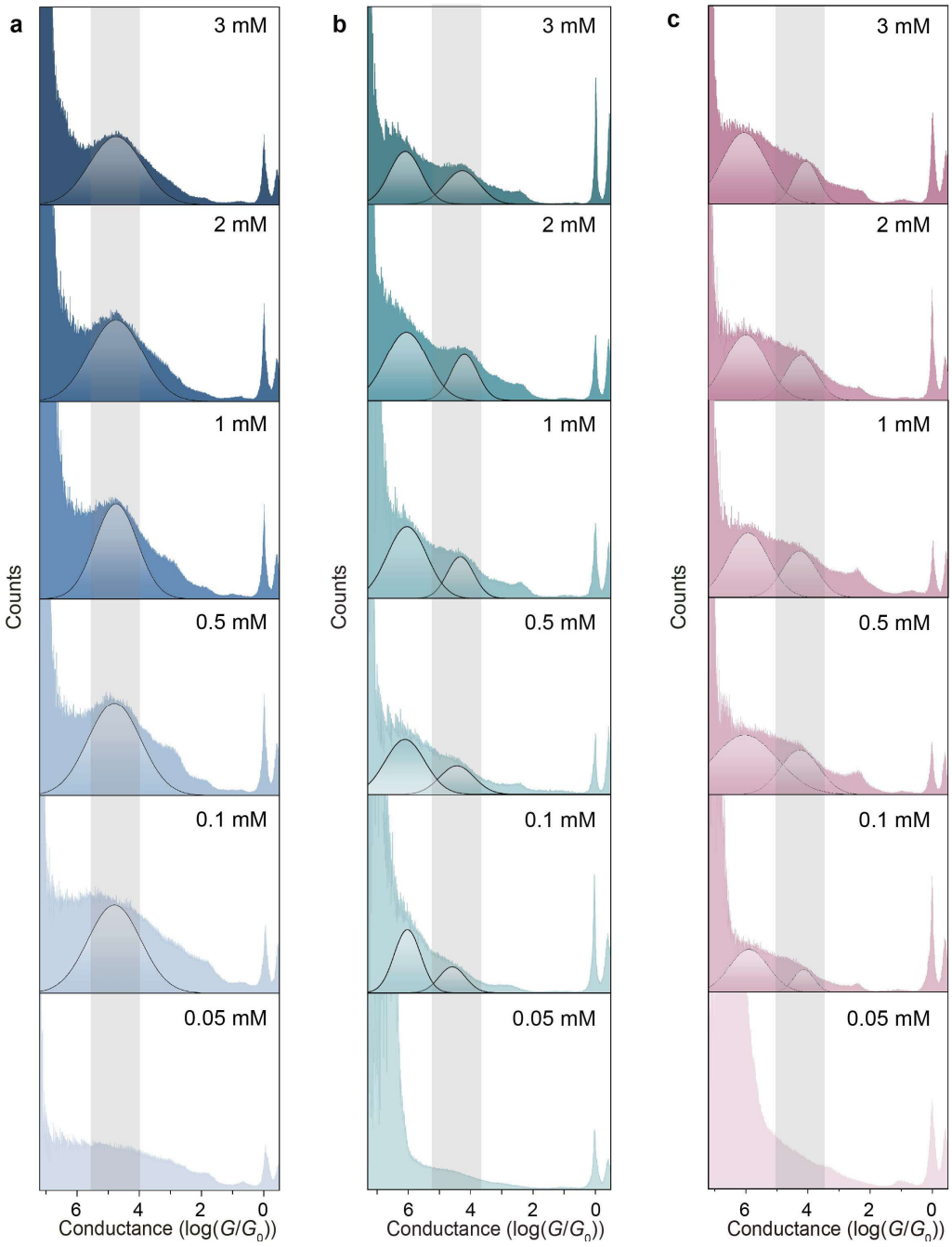

Supplementary Fig. 25 | Conductance measurements of the three DASAs with different molecular concentrations in dark. 1D conductance histograms of **a**, D1 **b**, D2 **c**, D3 at different concentrations (0.05-3.0 mM). The gray shaded regions highlight the conductance peaks associated with π-π stacking-induced supramolecular junctions. The conductance peak positions were determined by Gaussian fitting.

To investigate the concentration dependence of π-π stacking-induced conductance, we performed a series of control measurements for D1-D3 spanning a broad concentration range (0.05-3.0 mM). The resulting conductance histograms (Supplementary Fig. 25) reveal that a minimum concentration of 0.5 mM is required to reliably facilitate the formation of π-π stacking-induced conductance peaks. The gradual disappearance of these peaks at lower concentrations. This concentration-dependent behavior indicates that a sufficient molecular concentration is required to reliably form π-stacked supramolecular junctions within the STM-BJ nanogap. The decrease in peak intensity at low concentrations suggests a reduced probability of intermolecular association, supporting the assignment of the observed conductance features to concentration-dependent intermolecular coupling.

4.6 2D conductance-distance histograms of DASAs under 635 nm laser

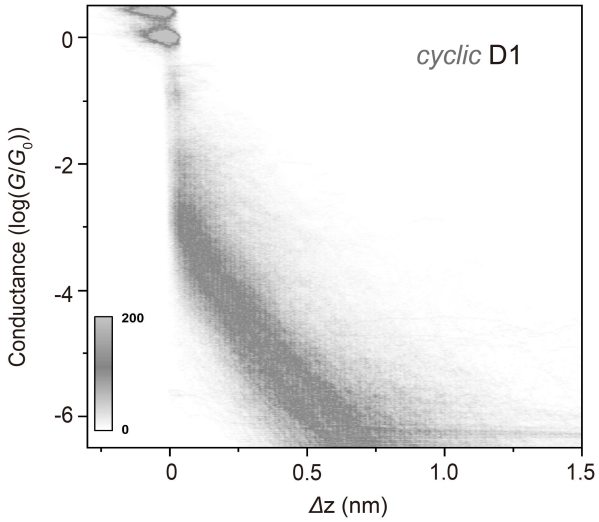

Supplementary Fig. 26 | 2D conductance histograms of D1 *homo*-junctions under 635 nm light irradiation. 2D conductance-distance histogram shows the disappearance of the D1-D1 π-stacked supramolecular junction feature.

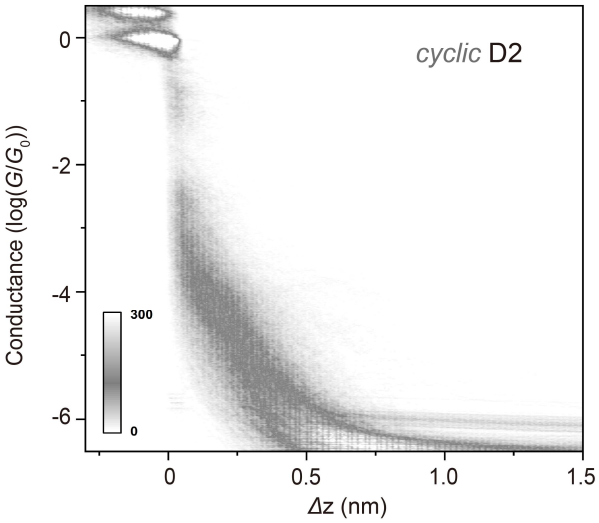

Supplementary Fig. 27 | 2D conductance histograms of D2 *homo*-junctions after 635 nm light irradiation. 2D conductance-distance histogram shows the disappearance of the D2-D2 π-stacked supramolecular junction feature.

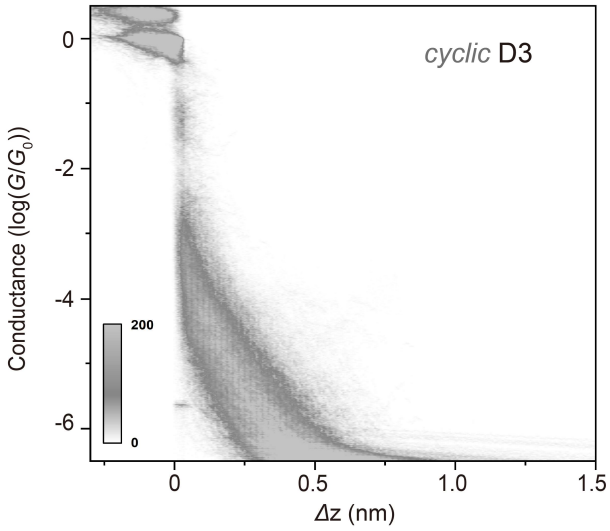

Supplementary Fig. 28 | 2D conductance histograms of D3 *homo*-junctions after 635 nm light irradiation. 2D conductance-distance histogram shows the disappearance of the D3-D3 π-stacked supramolecular junction feature.

The absence of distinct molecular conductance plateaus in the range from 10^{-1} G_0 to $10^{-6.5}$ G_0 indicates that 635 nm irradiation induces *linear*-to-*cyclic* isomerization of DASAs (Supplementary Figs. 26-28), thereby disrupting the π-stacked supramolecular junctions. The resulting *cyclic* isomers are electrically "OFF", or their conductance is below the detection limit of the STM-BJ setup. The density plots mainly show the characteristic exponential tunneling decay associated with the solvent background and gold electrode stretching.

4.7 Reversible conductance switching of DASAs *homo*-junctions

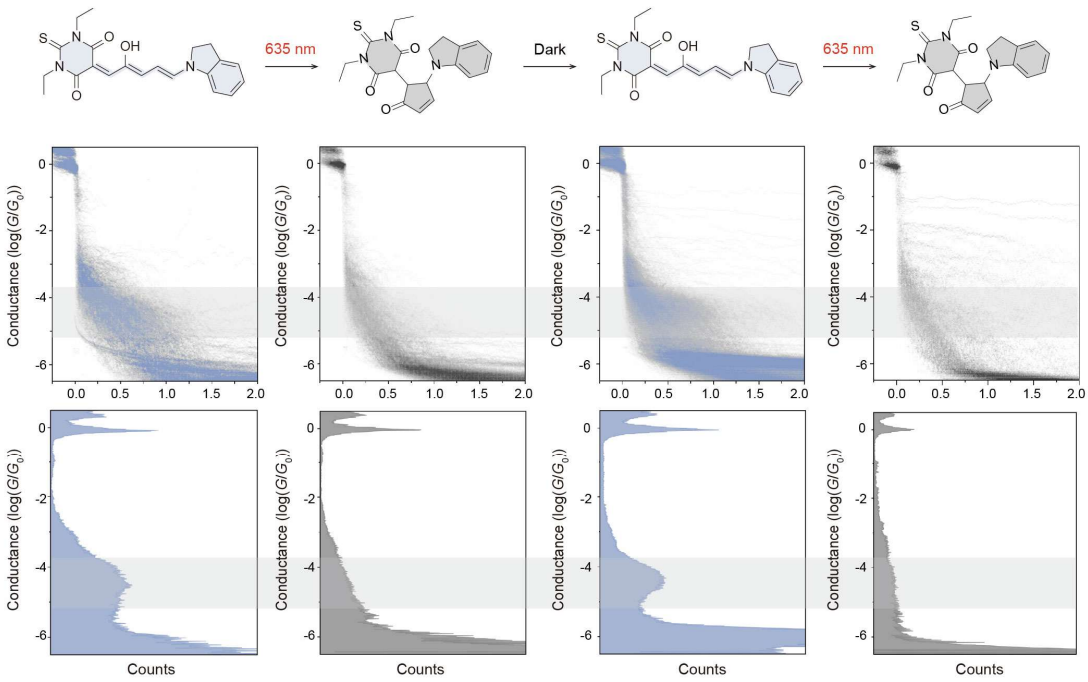

Supplementary Fig. 29 | Reversible conductance switching of D1-D1 supramolecular junctions. 2D conductance-distance histograms and corresponding 1D logarithmic conductance histograms of D1 recorded during repeated "light/dark" switching cycles. The conductance feature of *linear* D1 disappears after 635 nm irradiation due to photoinduced disassembly of the π-stacked supramolecular junction and recovers after thermal relaxation in the dark, confirming reversible photogated conductance modulation.

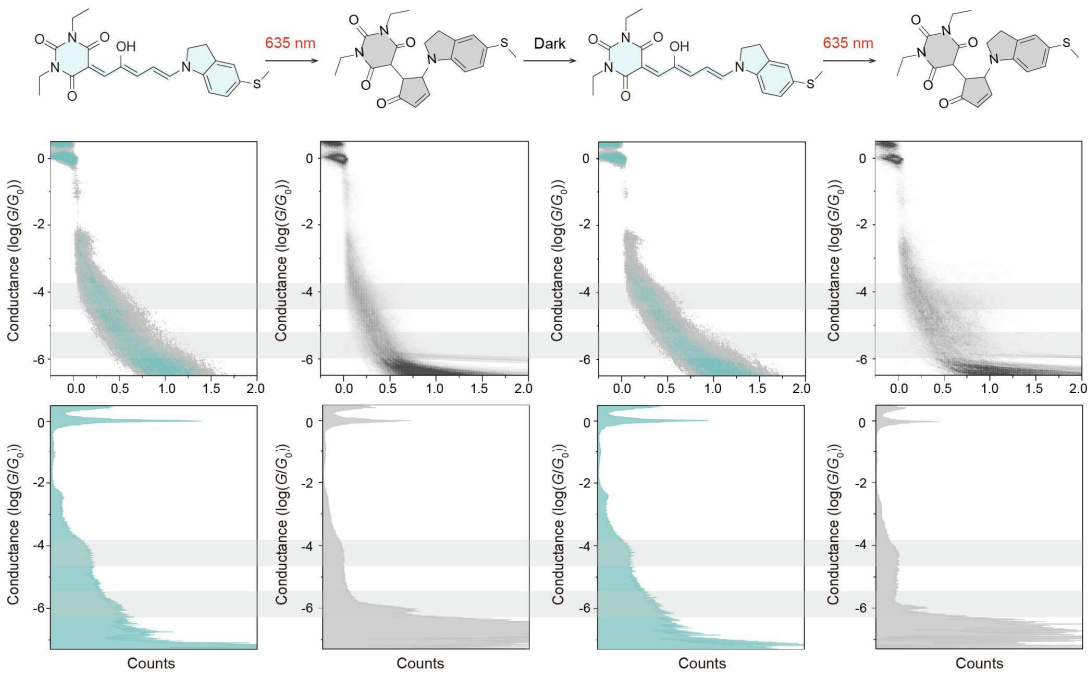

Supplementary Fig. 30 | Reversible conductance switching of D2-D2 supramolecular junctions. 2D conductance-distance histograms and corresponding 1D logarithmic conductance histograms of D2 recorded during repeated "light/dark" switching cycles. The conductance feature of *linear* D2 disappears after 635 nm irradiation due to photoinduced disassembly of the π-stacked supramolecular junction and recovers after thermal relaxation in the dark, confirming reversible photogated conductance modulation.

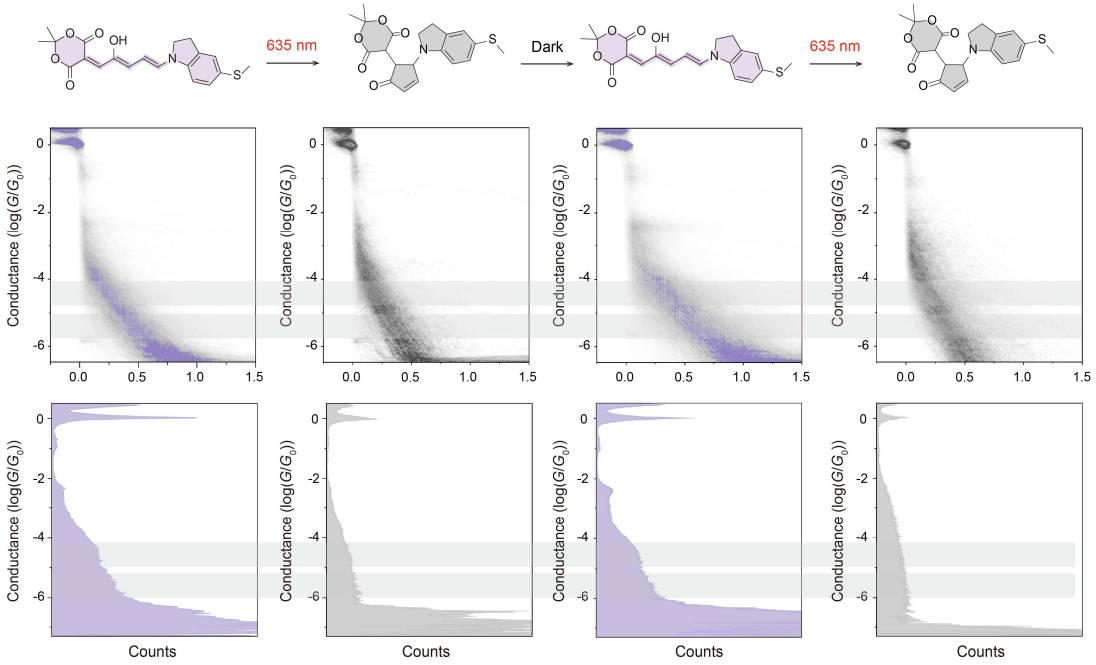

Supplementary Fig. 31 | Reversible conductance switching of D3-D3 supramolecular junctions. 2D conductance-distance histograms and corresponding 1D logarithmic conductance histograms of D3 recorded during repeated "light/dark" switching cycles. The conductance feature of *linear* D3 disappears after 635 nm irradiation due to photoinduced disassembly of the π-stacked supramolecular junction and recovers after thermal relaxation in the dark, confirming reversible photogated conductance modulation.

4.8 Transmission calculation analysis

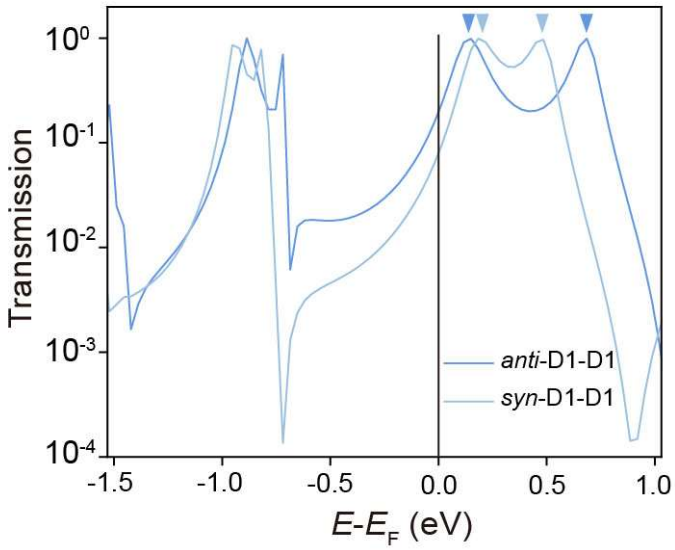

Supplementary Fig. 32 | Calculated transmission spectra of *anti*-D1-D1 and *syn*-D1-D1.

To understand why D1-D1 experimentally shows only one dominant conductance state, two hydroxyl-orientation-dependent D1-D1 conformations were examined by DFT and quantum transport calculations. As shown in Supplementary Fig. 17, both *anti*-D1-D1 and *syn*-D1-D1 exhibit intermolecular LUMO overlap across the π-stacked interface, indicating effective electronic coupling between the two *linear* D1 molecules. *anti*-D1-D1 shows a π-π distance of 3.33 Å and a binding energy of -36.20 kcal/mol, whereas *syn*-D1-D1 shows a slightly larger π-π distance of 3.46 Å and a weaker binding energy of -34.13 kcal/mol. The small binding-energy difference of 2.07 kcal/mol suggests that both conformations are energetically accessible. In contrast, the HOMO orbitals show almost no intermolecular overlap (Supplementary Fig. 17), indicating that intermolecular transport is mainly governed by the LUMO channel. Accordingly, both conformations exhibit similar LUMO-dominated transmission features near the Fermi level (Supplementary Fig. 32), suggesting that hydroxyl-orientation variation has only a limited influence on the D1-D1 transport pathway. This result explains why only one dominant D1-D1 conductance state is observed experimentally.

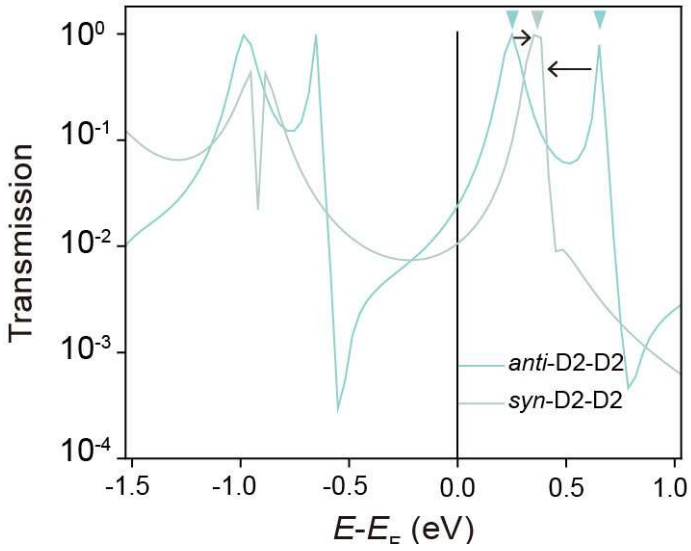

Supplementary Fig. 33 | Calculated transmission spectra of *anti*-D2-D2 and *syn*-D2-D2.

For comparison, D2-D2 was also examined by theoretical calculations. As shown in Supplementary Fig. 18, both *anti*-D2-D2 and *syn*-D2-D2 show intermolecular LUMO overlap across the π-stacked interface, confirming electronic coupling between the two *linear* D2 molecules. *anti*-D2-D2 has a shorter π-π distance of 3.30 Å and a stronger binding energy of -40.31 kcal/mol, whereas syn-D2-D2 has a larger π-π distance of 3.47 Å and a weaker binding energy of -37.35 kcal/mol. The HOMO orbitals are mainly localized on individual D2 molecules and show no obvious intermolecular overlap (Supplementary Fig. 18), indicating that transport is mainly governed by the LUMO channel. Compared with *anti*-D2-D2, *syn*-D2-D2 exhibits reduced transmission near the Fermi level because its larger π-π distance and altered stacking registry weaken the LUMO overlap and narrow the LUMO-derived transmission resonance (Supplementary Fig. 33). Thus, the packing geometry of D2-D2 can modulate intermolecular electron transport.

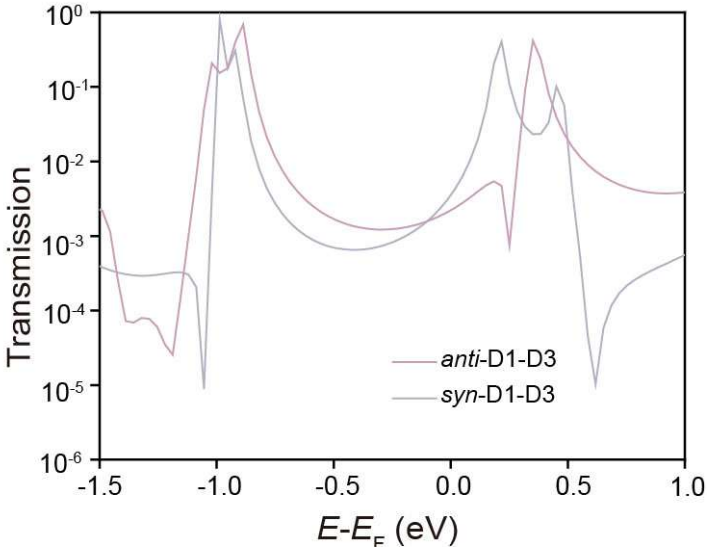

Supplementary Fig. 34 | Calculated transmission spectra of *anti*-D1-D3 and *syn*-D1-D3.

To understand the influence of hydroxyl orientation on the electronic properties of the D1-D3 *hetero*-junction, DFT and transmission calculations were performed for the *anti*-D1-D3 and *syn*-D1-D3 configurations (Supplementary Fig. 20). Both configurations exhibit stable π-stacked structures with a small binding-energy difference ($\Delta E_{binding}$ = -3.06 kcal/mol), suggesting that the two packing motifs are energetically accessible. The frontier molecular orbital distributions reveal distinct spatial characteristics between the two configurations, indicating that hydroxyl orientation modulates the intermolecular orbital arrangement and electronic coupling within the π-stacked interface. However, the calculated transmission spectra show closely transmission value near the Fermi level, with both configurations exhibiting LUMO-dominated transport characteristics (Supplementary Fig. 34). These results indicate that although hydroxyl orientation alters the local frontier orbital distribution, it does not substantially modify the dominant transport pathway of the D1-D3 *hetero*-junction. The similar transmission characteristics of the two configurations are consistent with the experimentally observed stable conductance behavior.

5. Orthogonality analysis of the D1/D3 mixture

The concentrations of *linear* D1 and D3 in the binary mixture were determined by multivariate spectral deconvolution using a non-negative least-squares fitting algorithm in MATLAB. Because the absorption spectra of D1 and D3 overlap strongly in the visible region, absorbance values at six representative wavelengths were simultaneously used for fitting rather than relying on a single-wavelength analysis.

The absorbance vector of the D1/D3 mixture was fitted using the calibrated absorption coefficients of D1 and D3 obtained from the standard curves in Section 3.1.1. The fitting was performed using the MATLAB function lsqnonneg, which solves the linear least-squares problem under a non-negative concentration constraint. This constraint ensures physically meaningful concentrations of *linear* D1 and D3 during the spectral deconvolution. The MATLAB code used for the concentration determination is shown below:

```
% Spectral deconvolution of the D1/D3 mixture by NNLS
% A = B*c, where c contains the concentrations of linear D1 and D3 in mM

A = [6.82 8.64 10.10 9.52 10.17 6.98]' / 10;

b_D1 = [1.34017 1.76298 2.16843 3.44512 6.26694 4.61223]';
b_D3 = [4.17554 5.12777 5.75174 3.77554 0.77917 0.34777]';

B = [b_D1 b_D3];
c = lsqnonneg(B, A);

A_fit = B * c;
RMSE = sqrt(mean((A - A_fit).^2));

fprintf('c_D1 = %.5f mM\n', c(1));
fprintf('c_D3 = %.5f mM\n', c(2));
fprintf('D1/D3 ratio = %.2f\n', c(1)/c(2));
fprintf('RMSE = %.5f Abs\n', RMSE);
```

The obtained concentrations of *linear* D1 and D3 were used to calculate the *linear*-to-*cyclic* isomerization conversions at different irradiation times. The same fitting

procedure was applied to all absorption spectra collected during the irradiation experiments.

6. D1 and D3 intermolecular interactions

6.1 ESI-MS evidence for intermolecular assembly of DASAs

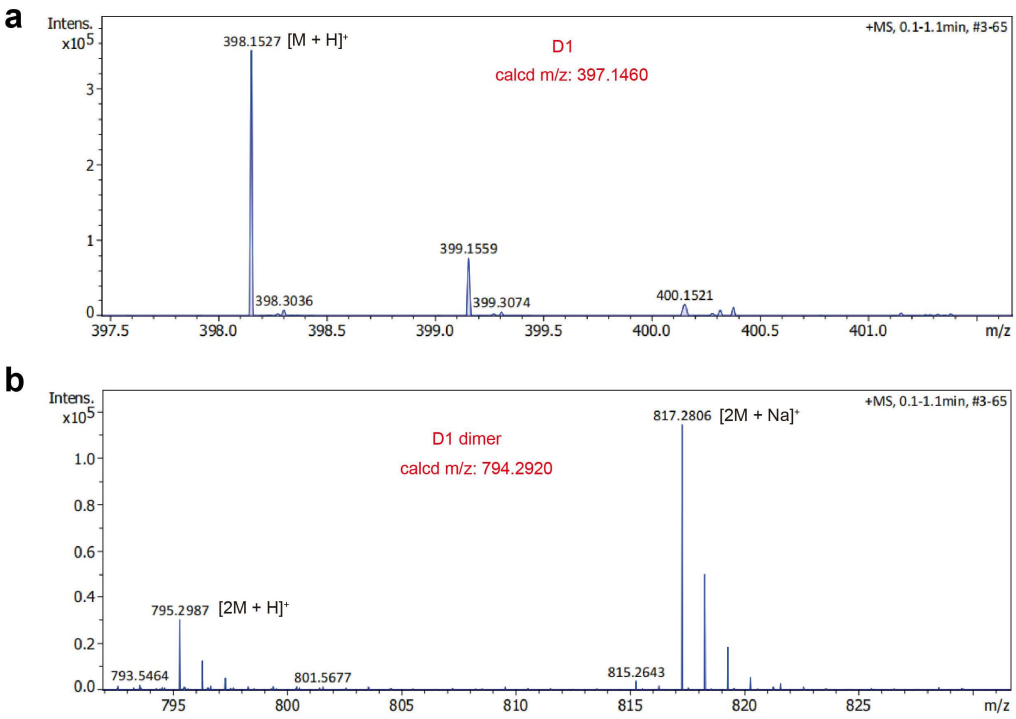

Supplementary Fig. 35 | Positive-ion ESI-MS spectra of D1. a, The mass spectrum of D1 shows a peak at *m*/z 398.1527, which is assigned to the protonated monomer [**M** + **H**]$^+$. **b**, The peaks at *m*/z 795.2987 and 817.2806 are assigned to the associated D1-D1 species [2**M** + **H**]$^+$ and [2**M** + **Na**]$^+$, respectively.

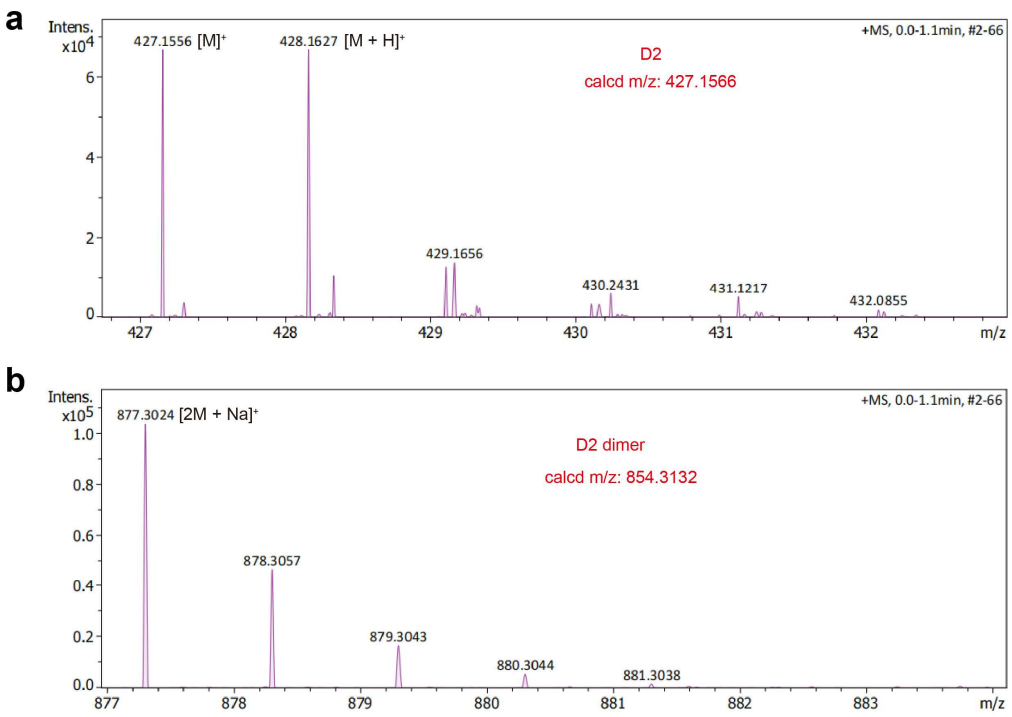

Supplementary Fig. 36 | Positive-ion ESI-MS spectra of D2. a, The mass spectrum of D2 displays two prominent peaks, a monomer peak $[\mathbf{M}]^+$ at *m*/*z* 427.1556 and a protonated monomer peak $[\mathbf{M} + \mathbf{H}]^+$ at *m*/*z* 428.1627. **b**, The peak at *m*/z 877.3024 corresponds to the sodium-adduct D2-D2 species $[2\mathbf{M} + \mathbf{Na}]^+$.

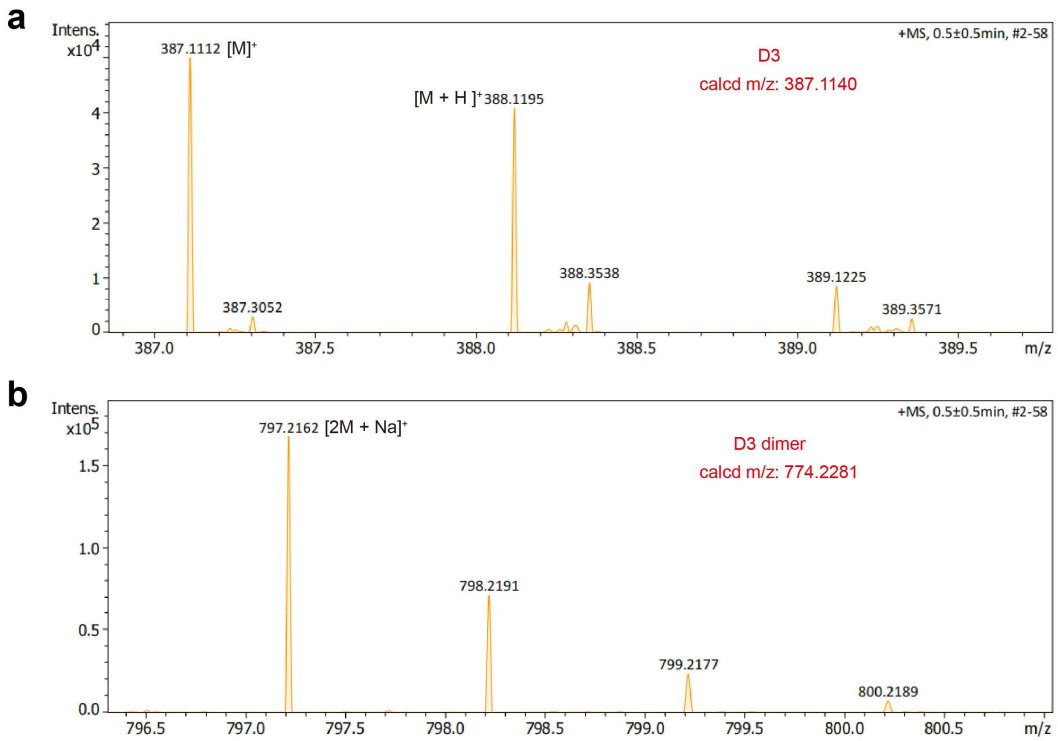

Supplementary Fig. 37 | Positive-ion ESI-MS characterization of D3. a, The mass spectrum of D3 exhibits two primary peaks, a monomer peak $[\mathbf{M}]^+$ at *m*/*z* 387.1112 and a protonated monomer peak $[\mathbf{M} + \mathbf{H}]^+$ at *m*/*z* 388.1195. **b**, The peak at *m*/z 797.2162 corresponds to the sodium-adduct D3-D3 species $[2\mathbf{M} + \mathbf{Na}]^+$.

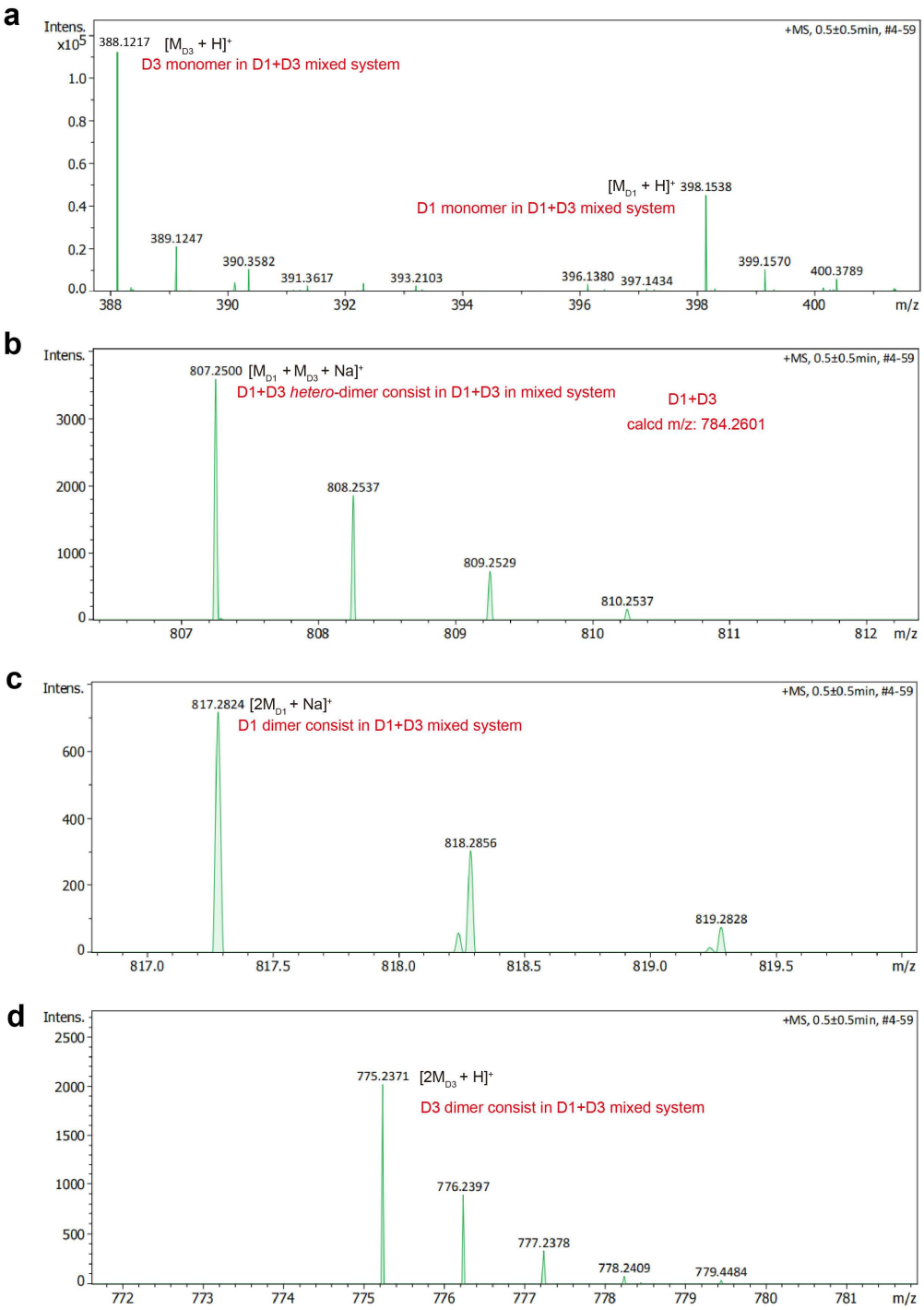

Supplementary Fig. 38 | Positive-ion ESI-MS spectra of D1 + D3 mixture. a, The mass spectrum of D1+D3 mixture exhibits a protonated D3 monomer peak $[\mathbf{M_{D3}} + \mathbf{H}]^+$ at *m*/*z* 388.1217 and a protonated D1 monomer peak $[\mathbf{M_{D1}} + \mathbf{H}]^+$ at *m*/*z* 398.1538. **b**, The peak at *m*/z 807.2500 corresponds to the sodium-adduct D1-D3 species $[\mathbf{M_{D1}} + \mathbf{M_{D3}} + \mathbf{Na}]^+$. **c,** The peak at *m*/z 817.2824 corresponds to the sodium-adduct D1-D1

species $[2\mathbf{M_{D1}} + \mathbf{Na}]^+$ in D1+D3 mixture. **d**, The peak at *m*/z 775.2371 corresponds to the protonated D3-D3 species $[2\mathbf{M_{D3}} + \mathbf{H}]^+$ in D1+D3 mixture.

The π-stacked dimer formation of DASA derivatives was investigated using electrospray ionization mass spectrometry (ESI-MS). For individual DASA derivatives, D1, D2 and D3 show not only monomer-related peaks but also higher-mass associated ion species, including protonated and/or sodium-adduct dimer signals (Supplementary Figs. 35-37). These results indicate that DASA molecules can form π-stacked *homo*-dimer species under the ESI-MS conditions, consistent with their tendency to undergo noncovalent intermolecular assembly.

In the D1+D3 binary mixture, in addition to the monomer peaks of D1 and D3 (Supplementary Fig. 38a), a distinct signal at m/z 807.2500 is observed and assigned to $[\mathbf{M_{D1}} + \mathbf{M_{D3}} + \mathbf{Na}]^+$ (Supplementary Fig. 38b). This signal supports the formation of a π-stacked D1-D3 *hetero*-dimer species, indicating that D1 and D3 can associate intermolecularly rather than existing only as isolated molecules.

6.2 UV-vis spectroscopic titration

To characterize the intermolecular π-π interactions between D1 and D3, UV-vis titration experiments were conducted in 1,1,2,2-tetrachloroethane. First, 3.0 mL of a 0.2 mM D3 solution was added to a quartz cuvette with a 0.5 mm path length. To maintain a constant D3 concentration and minimize dilution effects, the titrant was prepared as a 2 mM D1 stock solution in the same 0.2 mM D3 solution. The titration was performed in 25 steps, increasing the D1:D3 molar ratio from 0 to 2.

To accurately determine the values of the spectroscopic shifts, a custom MATLAB-based algorithm was developed to perform fitting analysis on the titration spectra. The

experimental spectrum of the mixed system, $A_{mix}(\lambda)$, was modeled as a linear superposition of the shifted spectra of the pure components:

$$A_{mix}(\lambda) = C_{D3} \cdot A_{pure}^{D3}(\lambda - \Delta\lambda_{D3}) + C_{D1} \cdot A_{pure}^{D1}(\lambda - \Delta\lambda_{D1}) \quad (1)$$

Where C represents the relative concentration coefficient, and $\Delta\lambda$ denotes the spectroscopic shift induced by intermolecular interactions. The fitting process utilized a dual grid-search method combined with constrained linear regression:

1. Shift Optimization: The search space for the shift of D3 was defined as a red shift (range: 0 to + 10 nm), while D1 was defined to undergo a blue shift (range: -10 to 0 nm), with a search precision of 0.05 nm.
2. Concentration Constraints: Given the constant substrate concentration method employed in this experiment, the algorithm strictly constrained the relative concentration coefficient of D3 (C_{D3}) within 0.982 ± 0.1 (initial concentration) to remain consistent with experimental conditions. Simultaneously, a non-negative least-squares regression was performed to determine the concentration of D1.
3. Result Determination: By iterating through all possible shift combinations, the optimal spectroscopic shift and component contributions for each titration point were determined by maximizing the coefficient of determination R^2. The MATLAB code used for the fitting analysis is shown below:

```
%% UV-vis spectral-shift fitting
clear; clc;

data = readmatrix('data.xlsx');
start_nm = 400; interval = 0.1;
[nSample,nPoint] = size(data);
wl = (start_nm:interval:start_nm+(nPoint-1)*interval)';

D3_0 = data(1,:)';
D1_0 = data(2,:)';

grid_D3 = 0:0.05:10;              % D3 red shift
grid_D1 = 0:-0.05:-10;            % D1 blue shift
```

```
D3_min = 0.982 - 0.100;
D3_max = 0.982 + 0.100;

results = zeros(nSample,5); % C_D3, C_D1, shift_D3, shift_D1, R2

for i = 1:nSample
    y = data(i,:)';
    bestR2 = -inf;

    for sD3 = grid_D3
        D3s = interp1(wl,D3_0,wl-sD3,'pchip',0);

        for sD1 = grid_D1
            D1s = interp1(wl,D1_0,wl-sD1,'pchip',0);

            c = [D3s,D1s]\y;
            C_D3 = min(max(c(1),D3_min),D3_max);
            C_D1 = max(sum(D1s.*(y-C_D3*D3s))/sum(D1s.^2),0);

            yfit = C_D3*D3s + C_D1*D1s;
            R2 = 1 - sum((y-yfit).^2)/sum((y-mean(y)).^2);

            if R2 > bestR2
                bestR2 = R2;
                results(i,:) = [C_D3,C_D1,sD3,sD1,R2];
            end
        end
    end
end

T = array2table(results,'VariableNames',{'C_D3','C_D1','Shift_D3_nm','Shift_D1_nm','R2'});
writetable(T,'Spectral_Shift_Fitting_Results.xlsx');
```

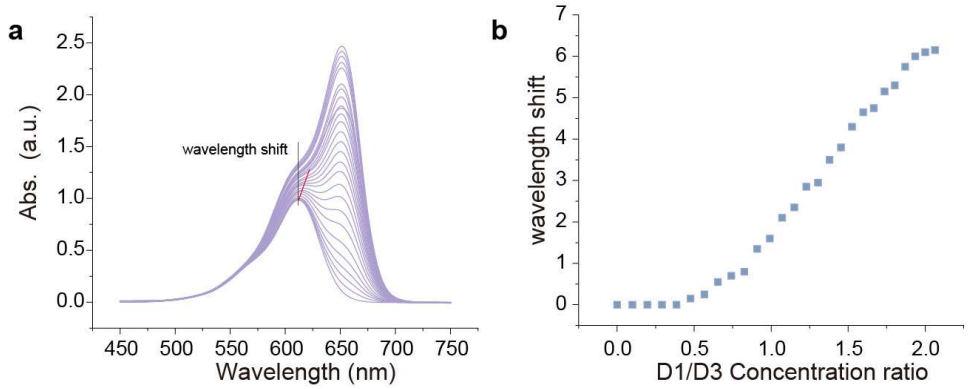

Supplementary Fig. 39 | UV-vis spectroscopic titration and peak shift analysis of the D1:D3 system. a, Evolution of the absorption spectra upon incremental addition of D1 to a constant concentration of D3 (0.2 mM). **b**, Plot of the peak wavelength shift as a function of the D1/D3 concentration ratio (from 0 to 2). The progressive shift substantiates the formation of heterosupramolecular D1:D3 assemblies in solution. The wavelength shift shows a sharp increase once the D1/D3 ratio reaches 1:1, marking the onset of effective intermolecular π-π coupling within the *hetero*-dimer structures.

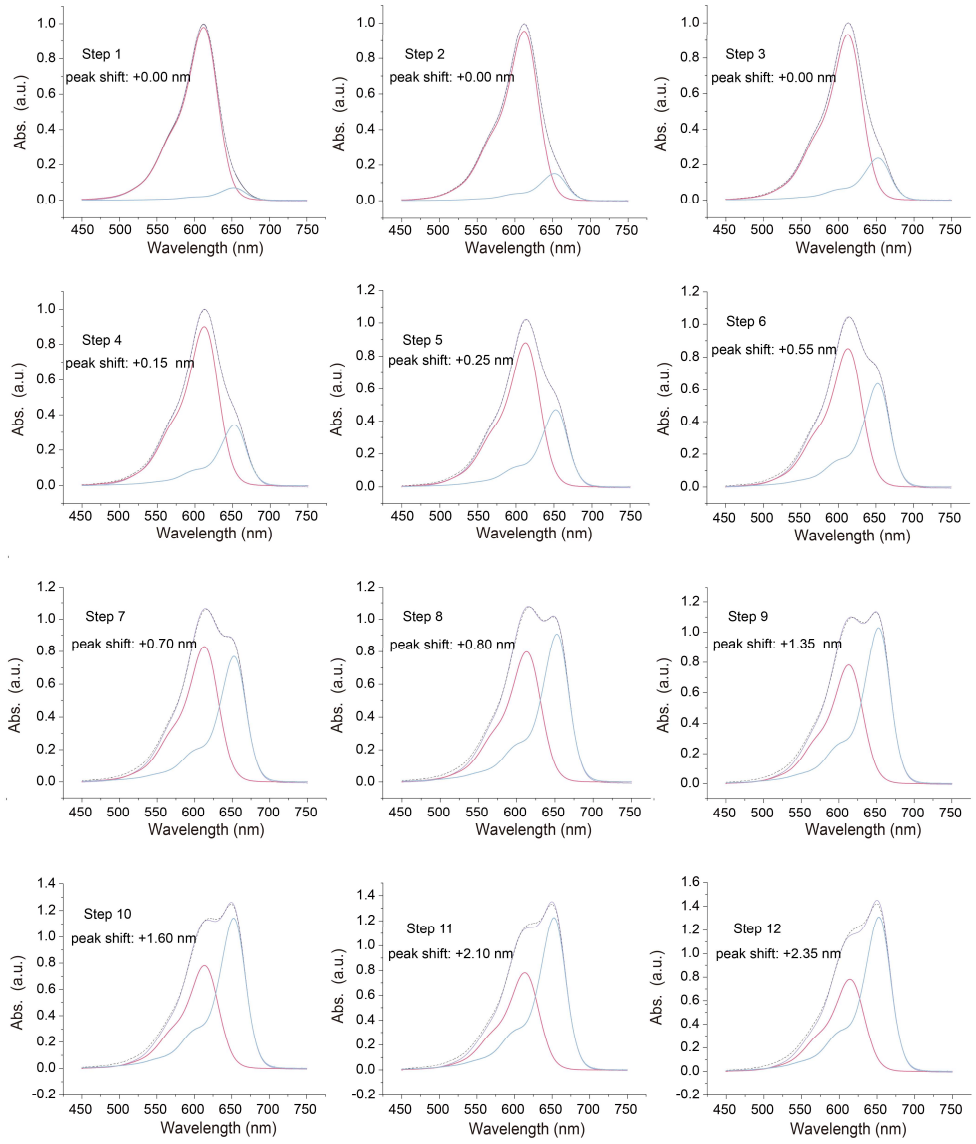

Supplementary Fig 40. | Spectral deconvolution and fitting results of the D1:D3 titration steps. Subplots from Step 1 to Step 12 illustrate the experimental absorption spectra (dotted lines) and the corresponding fitted component spectra (solid lines) representing D1 and D3 across the titration range. The "peak shift" values indicated in each Fig the calculated shift of the D3 absorption peak determined by the custom MATLAB fitting algorithm, the R^2 for each fitting step above 0.99.

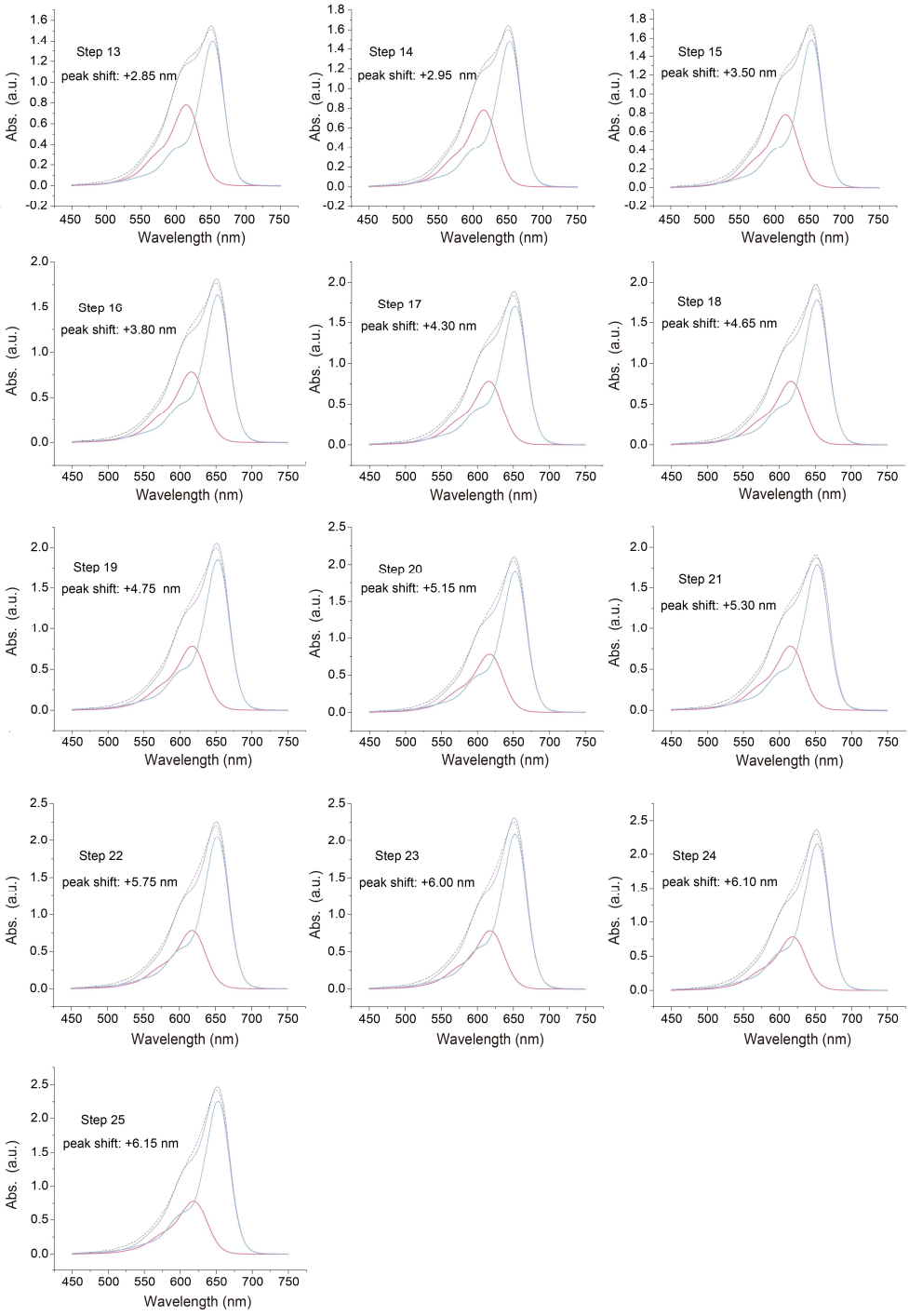

Supplementary Fig 41. | Spectral deconvolution and fitting results of the D1:D3 titration steps. Subplots from Step 13 to Step 25 illustrate the experimental absorption spectra (dotted lines) and the corresponding fitted component spectra (solid lines) representing D1 and D3 across the titration range. The “peak shift” values indicated in

each Fig the calculated shift of the D3 absorption peak determined by the custom MATLAB fitting algorithm, the R^2 for each fitting step above 0.99.

6.3 ^{1}H NMR titration and 2D NOESY

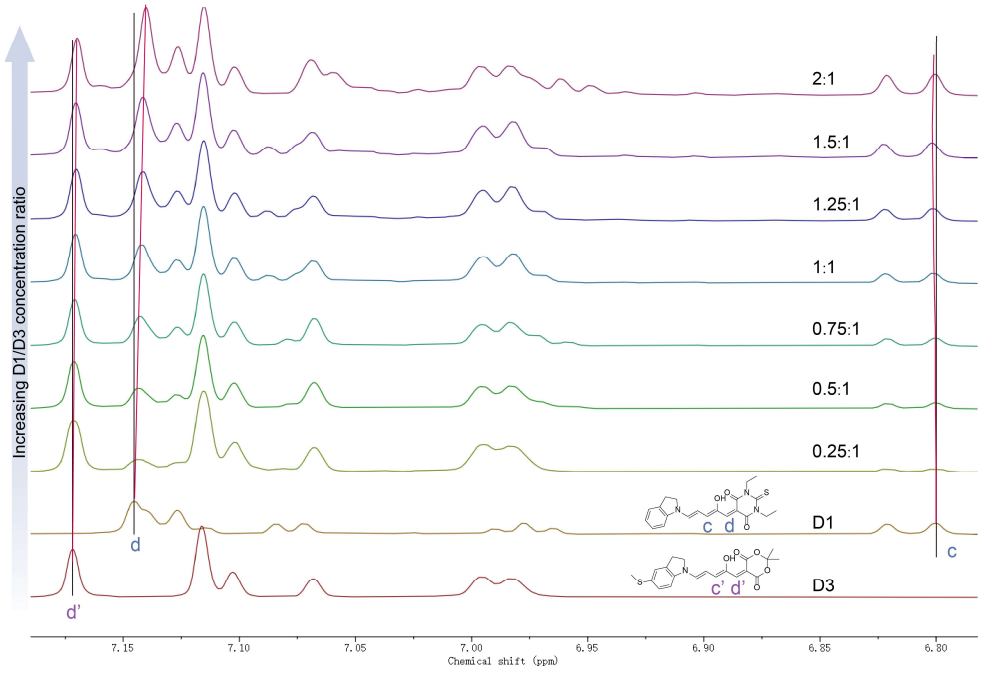

Supplementary Fig. 42 | ^{1}H NMR titration experiment of D3 with increasing amounts of D1. Stacked ^{1}H NMR spectra of D1/D3 mixtures obtained by gradually increasing the D1/D3 concentration ratio while keeping the D3 concentration constant at 8.6 mM.

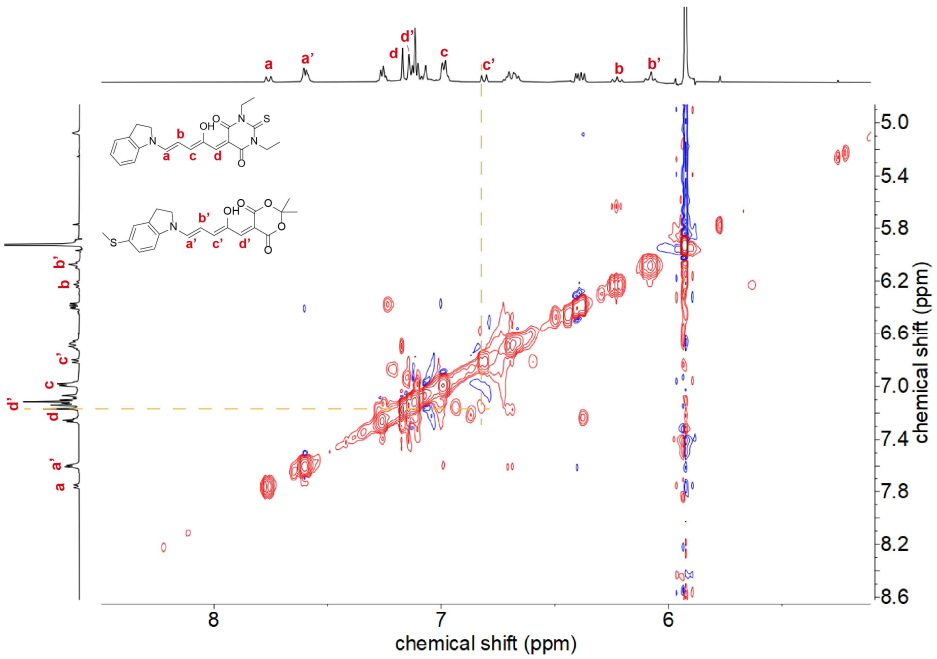

Supplementary Fig. 43 | 2D-NOESY spectrum of the D1 + D3 mixture at 1:1 molar ratio in $C_2D_2Cl_4$.

As shown in Supplementary Fig. 42, the proton signals of the D1/D3 mixture show clear concentration-dependent changes with increasing D3/D1 ratio. These changes mainly occur in the π-bridge region of 6.8-7.2 ppm, especially for the assigned π-bridge protons c/d of D1 and d′ of D3. The gradual shift and broadening of these resonances indicate that the local environments of the D1 and D3 π-bridges are affected after mixing, suggesting intermolecular association rather than independent coexistence in solution.

To further examine their spatial proximity, 2D-NOESY NMR measurements were performed for the D1+D3 mixture at a 1:1 molar ratio. As shown in Supplementary Fig. 43, additional NOESY cross-correlations appear in the π-bridge region after mixing D1 and D3. Correlations involving the π-bridge protons of D1 and D3, such as d, c′, and neighboring π-bridge resonances, indicate that their conjugated segments are spatially close in solution. Based on the above results, the concentration-dependent ^{1}H NMR perturbations and 2D-NOESY correlations suggest that D1 and D3 form

supramolecular assemblies through intermolecular π-π interactions. In this assembly, D1 and D3 most likely adopt a parallel stacking arrangement, in which the donor and acceptor units of the two DASA molecules are oriented in the same direction, allowing their conjugated π-bridges to approach each other.

Together with the UV-vis titration and ESI-MS results, the concentration-dependent ^{1}H NMR perturbations and NOESY correlations suggest that D1 and D3 form supramolecular assemblies in solution through intermolecular π-π interactions with a parallel stacking arrangement.

6.4 DFT analysis of D1+D3 interactions

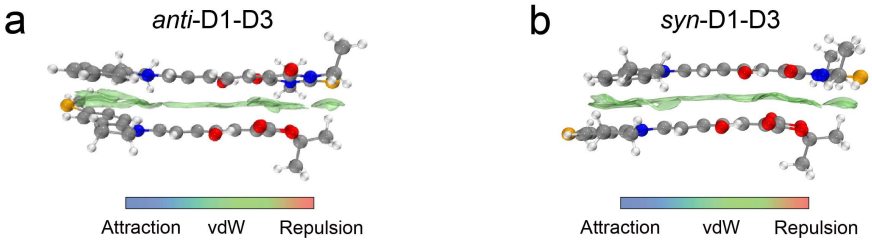

Supplementary Fig. 44 | IGM analysis of the D1-D3. IGM isosurfaces of **a**, *anti*-D1-D3 and **b**, *syn*-D1-D3 configurations, respectively[8].

The IGM analysis further reveals broad and continuous isosurfaces spanning the intermolecular region of both *anti*-D1-D3 and *syn*-D1-D3 configurations, with interaction characteristics dominated by van der Waals interactions (Supplementary Fig. 44)[9]. These extended green isosurfaces between the two molecular planes support the formation of π-π stacked D1-D3 *hetero*-assemblies.

6.5 PSD of D1-D3 *hetero*-junction

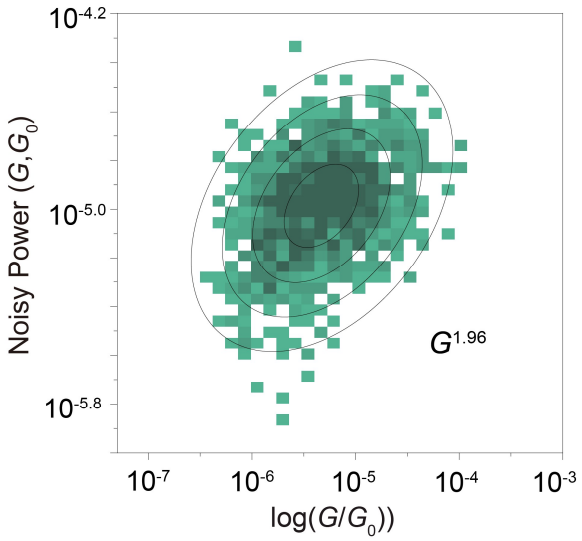

Supplementary Fig. 45 | PSD of the D1-D3 *hetero*-junction. The flicker-noise analysis of the D1-D3 *hetero*-junction gives a scaling exponent of $G^{1.96}$, close to the characteristic value of through-space transport[4, 5]. This result supports that the conductance of the D1-D3 supramolecular junction is primarily governed by intermolecular electron transport through the π-π stacked interface.

7. NMR spectra

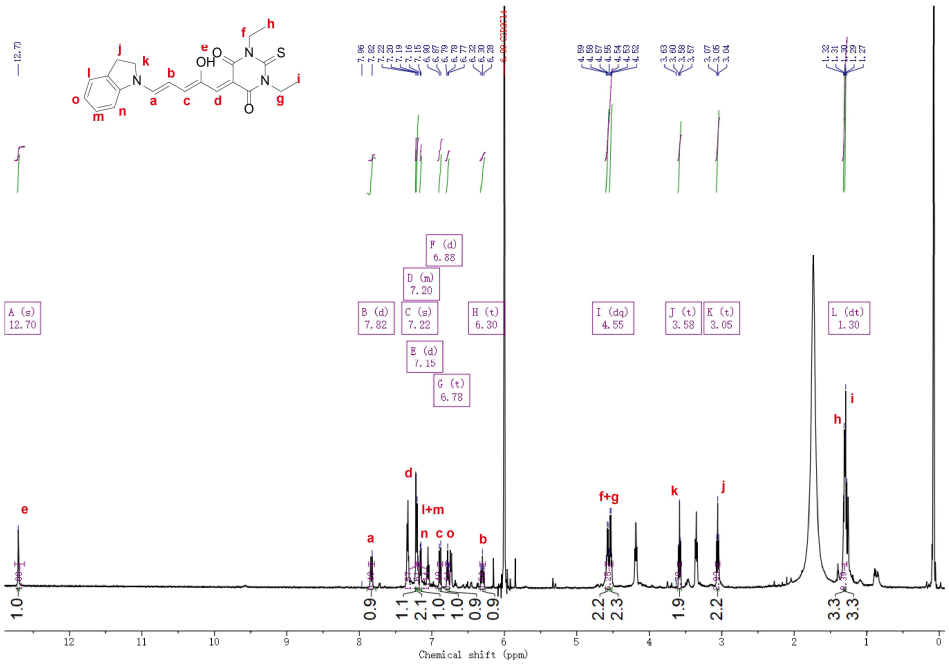

Supplementary Fig. 46 | ^{1}H NMR spectrum of D1 (600 MHz), solvent: $C_2D_2Cl_4$.

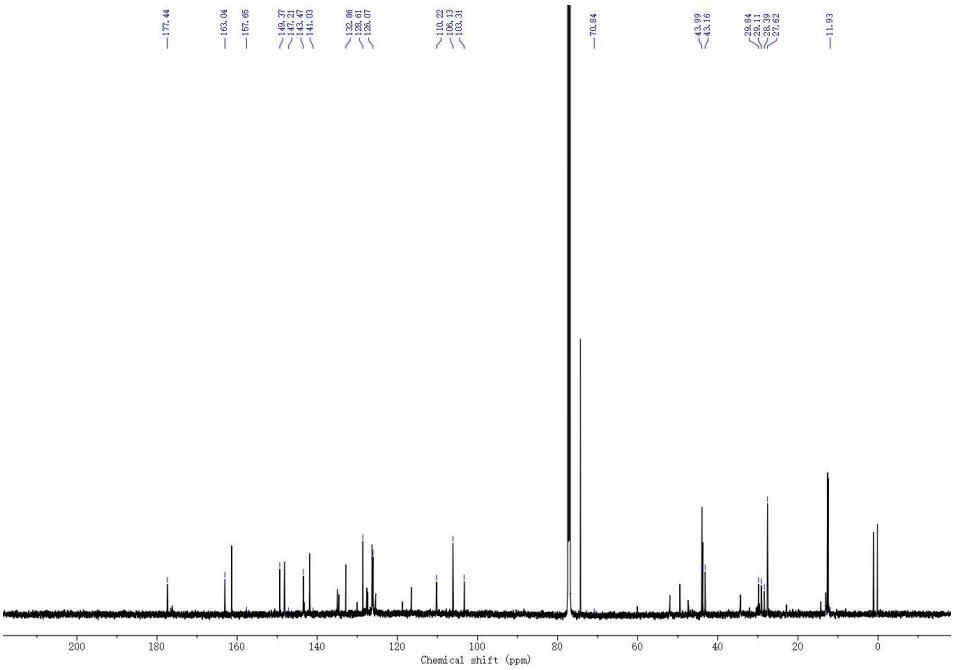

Supplementary Fig. 47 | ^{13}C NMR spectrum of D1 (151 MHz), solvent: $CDCl_3$.

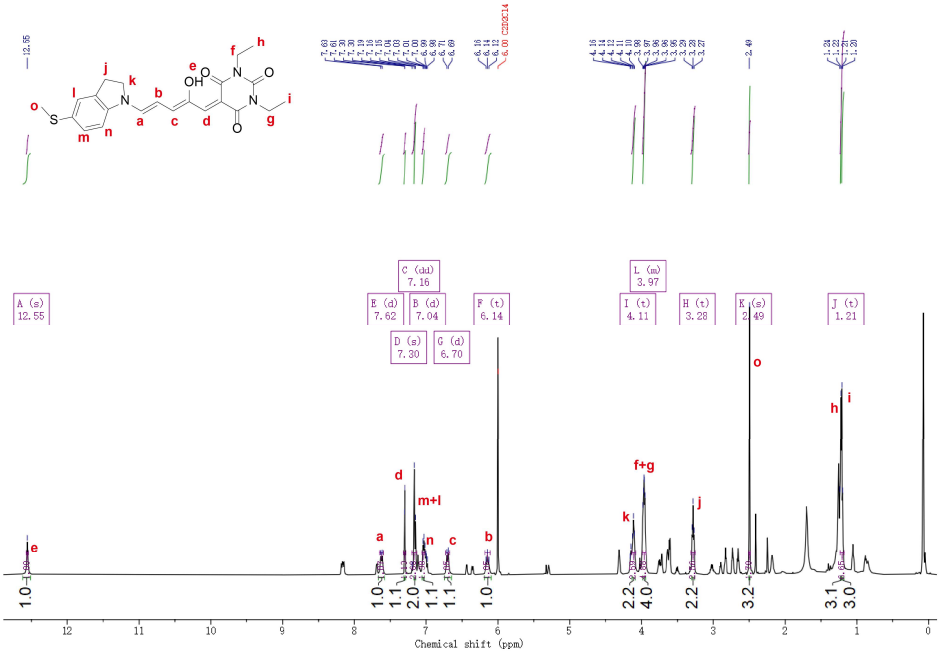

Supplementary Fig. 48 | ^{1}H NMR spectrum of D2 (600 MHz), solvent: $C_2D_2Cl_4$.

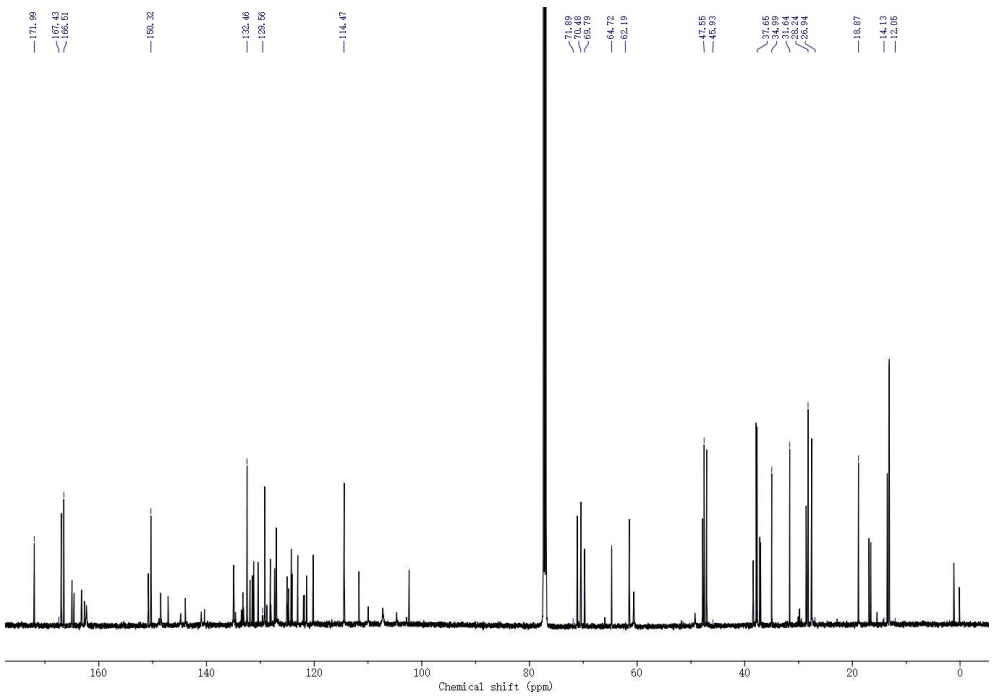

Supplementary Fig. 49 | ^{13}C NMR spectrum of D2 (151 MHz), solvent: $CDCl_3$.

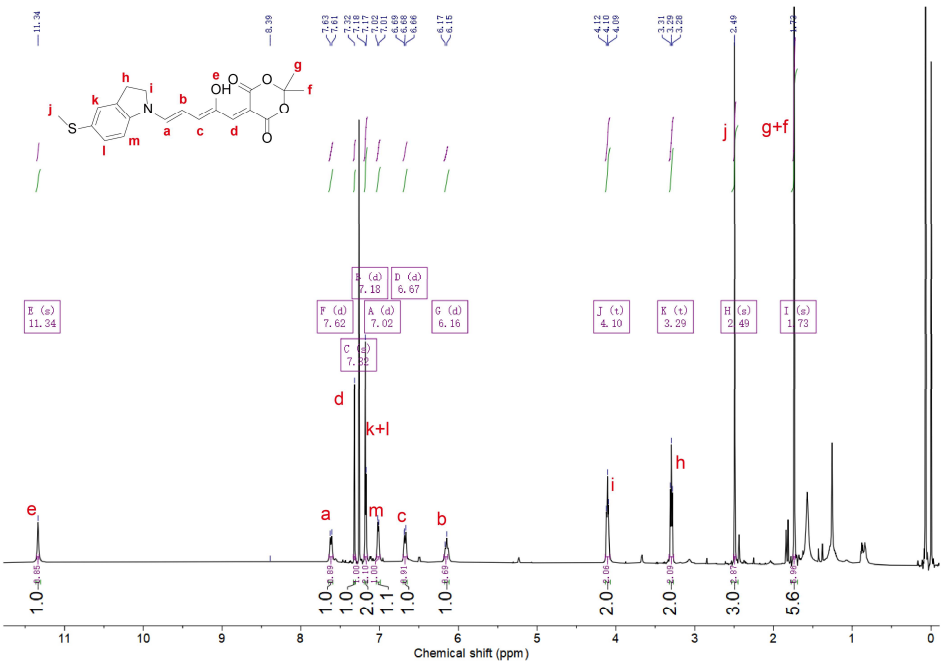

Supplementary Fig. 50 | ^{1}H NMR spectrum of D3 (600 MHz), solvent: $CDCl_3$.

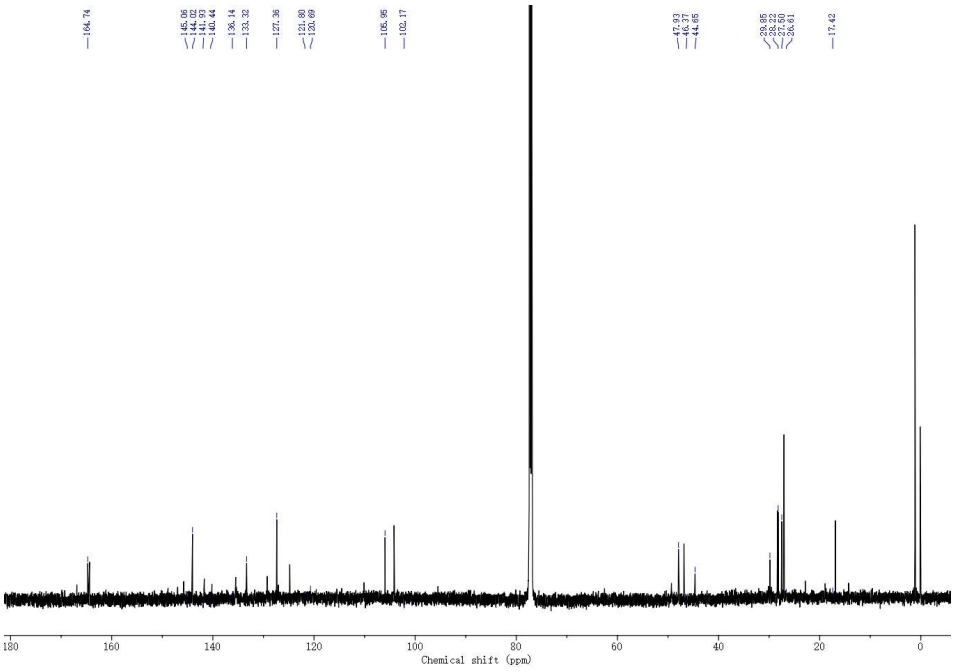

Supplementary Fig. 51 | ^{13}C NMR spectrum of D3 (151 MHz), solvent: $CDCl_3$.

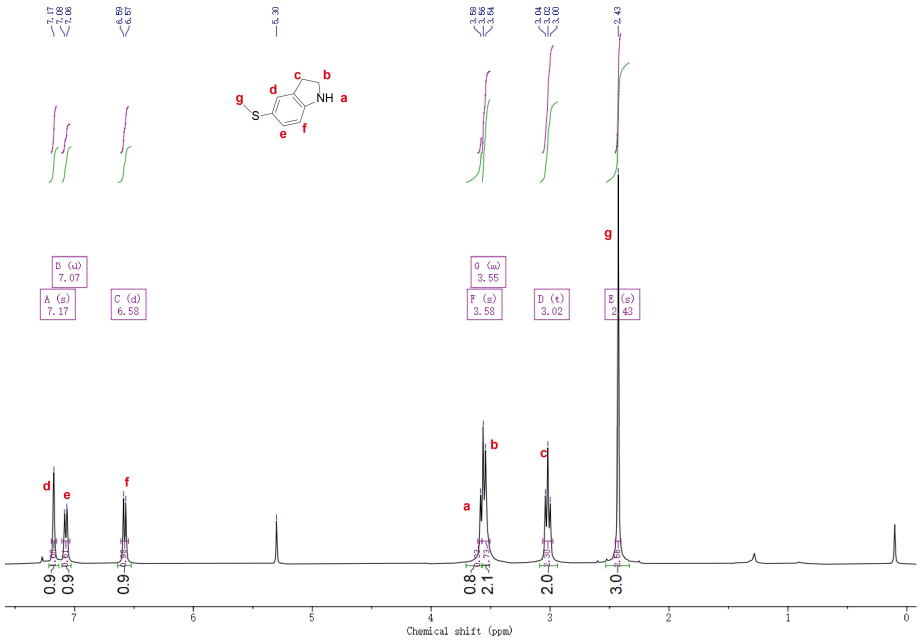

Supplementary Fig. 52 | ^{1}H NMR spectrum of 5-(methylthio)indoline (compound 6) (400 MHz), solvent: CD_2Cl_2.

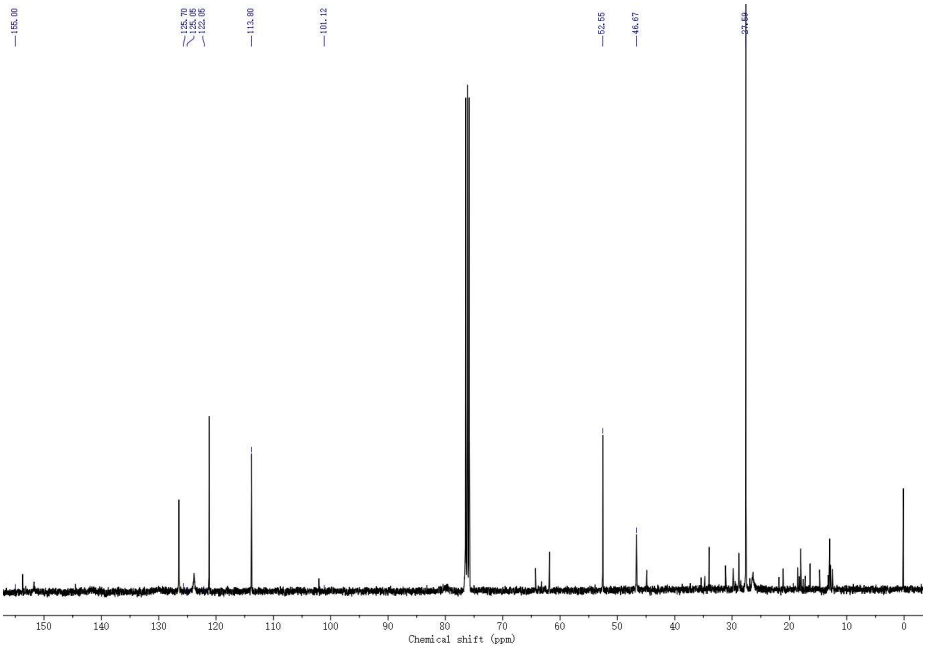

Supplementary Fig. 53 | ^{13}C NMR spectrum of 5-(methylthio)indoline (compound 6) (101 MHz), solvent: $CDCl_3$.

8. Cartesian coordinates

Supplementary Table 1. Cartesian coordinates of optimized *anti*-D1-D1 in Gaussian package.

C	4.07563886	1.01678687	-1.99747334
C	4.29467625	-0.11572240	-2.76996100
H	3.49731503	-0.80839069	-3.01633530
C	5.60001305	-0.36714039	-3.19064453
H	5.80002342	-1.24961405	-3.79003990
C	6.64822126	0.47684779	-2.83124996
C	6.40732962	1.60156868	-2.04040905
H	7.22824927	2.24558571	-1.73946741
C	5.11306256	1.87110562	-1.62823675
C	4.57753081	3.00995564	-0.79693488
H	4.66602209	3.96013960	-1.33426365
H	5.10172673	3.11442883	0.15590371
C	3.10115159	2.62885112	-0.56673962
H	2.92436676	2.32545494	0.47006523
H	2.40738006	3.43447159	-0.82190382
C	1.65095872	0.96048940	-1.67545087
H	1.62899192	0.12327438	-2.36642507
C	0.47692358	1.38582379	-1.09570428
H	0.46604839	2.17804187	-0.35574196
C	-0.73250740	0.76549824	-1.43098887
H	-0.72103429	-0.01590347	-2.18642148
C	-1.95875237	1.06569479	-0.84308438
C	-3.07753687	0.37606611	-1.32134764
H	-2.85051432	-0.37210469	-2.07626274
C	-4.44075624	0.41586927	-1.00569522
C	-5.07600766	1.42938906	-0.21505787
C	-7.24983526	0.32073520	-0.54280720
C	-5.23484101	-0.65733364	-1.56801886
C	-7.06712110	2.39919706	0.78276128
H	-6.30951195	2.71022206	1.49938068
H	-7.91288673	1.97150213	1.31672666
C	-7.49716053	3.57178662	-0.08770115
H	-8.24565741	3.25720248	-0.82016920
H	-6.63557435	3.99787811	-0.60930225
H	-7.93902719	4.35217795	0.53988773
C	-7.38419124	-1.75701315	-1.87298130
H	-6.70666429	-2.60842990	-1.92169194
H	-8.20695524	-1.98213166	-1.19681748
C	-7.89335385	-1.41255299	-3.26609354
H	-8.45361470	-2.25989479	-3.67364419
H	-7.05503871	-1.20095635	-3.93585416
H	-8.55872857	-0.54563742	-3.23169932
N	2.85924924	1.48050561	-1.45560310
N	-6.45750208	1.31764188	-0.01254351
N	-6.61274215	-0.65088510	-1.28056531
O	-1.95252239	1.93975013	0.18755971
H	-2.88343240	2.25294568	0.32066648
O	-4.49867398	2.41255878	0.27099691
O	-4.76725109	-1.56988696	-2.24425648
C	-4.07494788	-1.00479364	2.00316326
C	-4.29141765	0.13359119	2.76765855
H	-3.49272180	0.82691090	3.00780573
C	-5.59601300	0.39016908	3.18756207
H	-5.79410426	1.27731404	3.78067190
C	-6.64591522	-0.45454639	2.83489582
C	-6.40764067	-1.58510041	2.05158458
H	-7.22996920	-2.22954866	1.75546679
C	-5.11415452	-1.85972260	1.64039209
C	-4.58091938	-3.00514035	0.81665040
H	-4.66791913	-3.95085181	1.36212716
H	-5.10790006	-3.11773104	-0.13375818
C	-3.10509606	-2.62597514	0.57983738
H	-2.93191829	-2.32695361	-0.45883826
H	-2.41089658	-3.43089761	0.83593213
C	-1.65025432	-0.95650676	1.68156745
H	-1.62615593	-0.11832150	2.37130448
C	-0.47751960	-1.38484696	1.10142965
H	-0.46904833	-2.17692911	0.36127638
C	0.73346281	-0.76691459	1.43559303
H	0.72451731	0.01343704	2.19214081
C	1.95820906	-1.06816012	0.84507905
C	3.07886664	-0.38093044	1.32252355
H	2.85421891	0.36538732	2.07997444
C	4.44145405	-0.42108763	1.00423404
C	5.07389095	-1.43106172	0.20682733
C	7.24997454	-0.32763332	0.53716562
C	5.23799670	0.64853200	1.57008724
C	7.06147557	-2.39752123	-0.80106800
H	6.30198339	-2.70254676	-1.51832176
H	7.90686020	-1.96769320	-1.33393084
C	7.49130418	-3.57651261	0.06077907
H	8.24177494	-3.26794504	0.79378430
H	6.63006334	-4.00462066	0.58129091
H	7.93063153	-4.35347325	-0.57282362
C	7.38955271	1.74332055	1.87738138
H	6.71399196	2.59605761	1.93001004
H	8.21234840	1.96954322	1.20163875
C	7.89901382	1.39177383	3.26859148
H	8.46133381	2.23616382	3.67941930
H	7.06080034	1.17893201	3.93807174
H	8.56259659	0.52366289	3.22982207
N	-2.85982204	-1.47427735	1.46347724
N	6.45514015	-1.32013991	0.00239116
N	6.61546122	0.64134024	1.28061466
O	1.94849101	-1.94084398	-0.18659912
H	2.87922538	-2.25228711	-0.32480987
O	4.49434007	-2.41063178	-0.28382659
O	4.77287696	1.55850932	2.25146484
H	-7.65867125	-0.22159936	3.14612161
H	7.66159077	0.24788344	-3.14341931
S	-8.90617232	0.28954214	-0.29431303
S	8.90621704	-0.29892403	0.28785330

Supplementary Table 2. Cartesian coordinates of optimized *syn*-D1-D1 in Gaussian package.

C	-4.27920785	-0.57435753	-2.17558130
C	-4.69202524	0.74272963	-2.33745574
H	-3.99996668	1.57647660	-2.27964310
C	-6.05059547	0.97509289	-2.54485674
H	-6.40073570	1.99645178	-2.65643716
C	-6.96249519	-0.07724415	-2.59539183
C	-6.52597074	-1.39198951	-2.42746279
H	-7.23610396	-2.21362662	-2.44946908
C	-5.18009411	-1.63675686	-2.20988351
C	-4.46576085	-2.93574359	-1.93460770
H	-4.62815625	-3.67253179	-2.72665359
H	-4.80909097	-3.37034383	-0.99136505
C	-2.98157258	-2.52553237	-1.83397899
H	-2.52618289	-2.80071678	-0.87933275
H	-2.37670490	-2.94613845	-2.64474238
C	-1.85692588	-0.33334894	-1.88137390
H	-1.99915638	0.74177596	-1.95148188
C	-0.58967884	-0.84317461	-1.73140448
H	-0.42003948	-1.91020533	-1.65000625
C	0.51387853	0.01625623	-1.62471363
H	0.34375673	1.08894768	-1.66956673
C	1.82081222	-0.41546808	-1.43462876
C	2.79600167	0.57767576	-1.26493203
H	2.40340033	1.59020464	-1.30618986
C	4.17262728	0.56792019	-1.02864661
C	5.01191328	-0.59551734	-0.99065326
C	6.99134593	0.84257023	-0.71225931
C	4.75973172	1.87750168	-0.79232394
C	7.21325588	-1.61501316	-0.86668638
H	6.62220929	-2.39877501	-0.39656762

H	8.09492841	-1.42183376	-0.25964862
C	7.59490058	-2.00692753	-2.28727902
H	8.17875887	-1.21394732	-2.76248538
H	6.70085551	-2.20682814	-2.88447722
H	8.20439894	-2.91590008	-2.26652017
C	6.70833331	3.27674292	-0.40006680
H	5.95226465	3.81555943	0.16990268
H	7.60667599	3.16147665	0.20388233
C	7.01038832	4.00528484	-1.70237158
H	7.40988619	5.00041503	-1.48296462
H	6.09739326	4.12437628	-2.29226913
H	7.75372614	3.45813762	-2.28845894
N	-2.97795427	-1.05901143	-1.94609663
N	6.38585349	-0.39547051	-0.83294444
N	6.15731485	1.93059832	-0.63221360
O	2.02793732	-1.74901466	-1.36916085
H	3.00442553	-1.90100950	-1.31374469
O	4.60906100	-1.76439544	-1.10807377
O	4.10843720	2.91175059	-0.72238256
C	4.27933673	-0.57233211	2.17601928
C	4.69230597	0.74479564	2.33720157
H	4.00036524	1.57860130	2.27883663
C	6.05087911	0.97709469	2.54464333
H	6.40114814	1.99847399	2.65563612
C	6.96262245	-0.07533877	2.59599737
C	6.52593957	-1.39012993	2.42883280
H	7.23595102	-2.21185448	2.45148824
C	5.18007340	-1.63484347	2.21112434
C	4.46561886	-2.93387317	1.93637623
H	4.80892185	-3.36884073	0.99327028
H	4.62791836	-3.67038473	2.72870088
C	2.98147642	-2.52353966	1.83554052
H	2.37658545	-2.94355646	2.64659425
H	2.52604757	-2.79920286	0.88105480
C	1.85715557	-0.33114068	1.88100702
H	1.99955763	0.74404001	1.94992305
C	0.58985616	-0.84096035	1.73141882
H	0.42010908	-1.90806528	1.65123551
C	-0.51366505	0.01838995	1.62371035
H	-0.34354423	1.09113430	1.66726665
C	-1.82061725	-0.41362082	1.43426801
C	-2.79597106	0.57923475	1.26385946
H	-2.40345897	1.59184740	1.30391790
C	-4.17270894	0.56907939	1.02816018
C	-5.01184560	-0.59451446	0.99136147
C	-6.99152903	0.84304636	0.71197294
C	-4.76004691	1.87837178	0.79082090
C	-7.21302585	-1.61446549	0.86820246
H	-8.09491021	-1.42177414	0.26131728
H	-6.62198317	-2.39835261	0.39827313
C	-7.59424662	-2.00566499	2.28910399
H	-6.70003650	-2.20504050	2.88622439
H	-8.17815836	-1.21251830	2.76397380
H	-8.20358263	-2.91476171	2.26900812
C	-6.70894975	3.27699154	0.39771322
H	-7.60742816	3.16100805	-0.20589966
H	-5.95309234	3.81537604	-0.17294467
C	-7.01078827	4.00670786	1.69940671
H	-7.41046209	5.00158406	1.47916411
H	-7.75391458	3.46001639	2.28618636
H	-6.09766790	4.12647252	2.28897612
N	2.97805223	-1.05693946	1.94666939
N	-6.38583582	-0.39481075	0.83351829
N	-6.15768560	1.93113317	0.63097120
O	-2.02765724	-1.74724096	1.37032060
H	-3.00415248	-1.89937363	1.31530905
O	-4.60885100	-1.76324757	1.10972716
O	-4.10891839	2.91264747	0.71979917
H	8.01710888	0.13165836	2.74171195
H	-8.01698119	0.12980885	-2.74103683
S	8.65648417	1.00256394	-0.65926269
S	-8.65670663	1.00276830	0.65912446

Supplementary Table 3. Cartesian coordinates of optimized *anti*-D2-D2 in Gaussian package.

C	-4.36765653	-1.72019174	0.68314884
C	-4.65855319	-2.31941915	-0.53622650
H	-3.88732856	-2.56130207	-1.25928679
C	-5.99166454	-2.56978123	-0.83951098
H	-6.23828654	-3.02267192	-1.79515671
C	-7.02269106	-2.22894785	0.04588717
C	-6.70537098	-1.61104518	1.26127745
H	-7.48138952	-1.32574516	1.96372181
C	-5.37827635	-1.36042707	1.56883307
C	-4.78310455	-0.74499498	2.81081435
H	-4.96822880	-1.37696096	3.68579379
H	-5.19142456	0.24609411	3.02347438
C	-3.27674464	-0.65562109	2.48779390
H	-2.95616843	0.38287443	2.35882475
H	-2.65017968	-1.12381899	3.25242868
C	-9.69489858	-1.59865992	0.62166972
H	-9.66957597	-1.93711272	1.66078755
H	-10.71696538	-1.70055802	0.24966290
H	-9.38763043	-0.55283296	0.53843809
C	-1.91898745	-1.64448680	0.67285926
H	-1.95215071	-2.19312289	-0.26365493
C	-0.70485525	-1.26852220	1.19226344
H	-0.63840296	-0.67100943	2.09444055
C	0.48636145	-1.61972114	0.53655328
H	0.42335582	-2.23337214	-0.35814065
C	1.74885402	-1.21186312	0.94524562
C	2.84092012	-1.67208567	0.19366426
H	2.56125667	-2.27117642	-0.66927183
C	4.22195493	-1.50126002	0.29065030
C	4.91081276	-0.90765246	1.41256587
C	7.05554651	-1.30648766	0.27955052
C	4.98229641	-1.99952511	-0.85023100
C	7.02853677	-0.26742604	2.47884139
H	6.37201371	0.47520449	2.92966137
H	7.91013146	0.23348880	2.07981129
C	7.41357418	-1.33936620	3.48971123
H	8.06638422	-2.08595055	3.02819879
H	6.52155962	-1.83527834	3.88347398
H	7.95207665	-0.88452085	4.32708354
C	7.17291178	-2.33861290	-1.91668277
H	6.53669525	-2.28305304	-2.79978336
H	8.01782718	-1.65875672	-2.03294386
C	7.65247125	-3.76734976	-1.69476914
H	8.24136959	-4.10348795	-2.55405991
H	6.79824037	-4.44068404	-1.57875204
H	8.28121399	-3.82530291	-0.80207409
N	-3.11183778	-1.37875143	1.21737588
N	6.29674570	-0.83007592	1.33631298
N	6.36979497	-1.84696056	-0.79361597
O	1.81680970	-0.34898203	1.98270175
H	2.75431680	-0.33064979	2.30172296
O	4.36394684	-0.49167104	2.44378923
O	8.27521487	-1.24915251	0.29162878
O	4.47201719	-2.50364630	-1.84740268
S	-8.67440952	-2.64245163	-0.45095086
C	4.36770447	1.72020878	-0.68297847
C	4.65865698	2.31936466	0.53642078
H	3.88746050	2.56123179	1.25951598
C	5.99178350	2.56965214	0.83968564
H	6.23844376	3.02250486	1.79534041
C	7.02278250	2.22878447	-0.04573868
C	6.70540622	1.61094862	-1.26114471
H	7.48139010	1.32560224	-1.96360795
C	5.37828789	1.36043538	-1.56869328
C	4.78306848	0.74509435	-2.81069973
H	4.96819671	1.37710681	-3.68564502
H	5.19136602	-0.24599178	-3.02339972
C	3.27671240	0.65575988	-2.48764603
H	2.95610665	-0.38273002	-2.35871903
H	2.65013946	1.12400556	-3.25224088
C	9.69496187	1.59882916	-0.62198423
H	9.66942113	1.93760793	-1.66099084
H	10.71707757	1.70073848	-0.25011694
H	9.38785300	0.55293321	-0.53904647
C	1.91902114	1.64464958	-0.67268254
H	1.95219673	2.19334234	0.26379865
C	0.70488795	1.26868771	-1.19208874

H	0.63845228	0.67112596	-2.09423435
C	-0.48635135	1.61992167	-0.53643865
H	-0.42339240	2.23365869	0.35819980
C	-1.74881247	1.21197894	-0.94514883
C	-2.84093816	1.67217934	-0.19364067
H	-2.56134549	2.27132720	0.66927828
C	-4.22196214	1.50129238	-0.29070103
C	-4.91073165	0.90766937	-1.41266462
C	-7.05554598	1.30648967	-0.27981123
C	-4.98239169	1.99954491	0.85012763
C	-7.02838781	0.26732637	-2.47904031
H	-6.37152602	-0.47484902	-2.93011135
H	-7.90968860	-0.23413928	-2.08003971
C	-7.41405272	1.33930625	-3.48962741
H	-8.06720762	2.08544825	-3.02790591
H	-6.52230539	1.83575864	-3.88333247
H	-7.95236034	0.88437549	-4.32707900
C	-7.17308910	2.33853915	1.91644289
H	-6.53696423	2.28295826	2.79960894
H	-8.01800176	1.65866316	2.03259762
C	-7.65265996	3.76727312	1.69453999
H	-8.24164297	4.10337028	2.55378952
H	-6.79843606	4.44063298	1.57861970
H	-8.28132544	3.82524330	0.80179111
N	3.11185565	1.37885688	-1.21720191
N	-6.29667024	0.83005299	-1.33650039
N	-6.36988117	1.84696476	0.79340975
O	-1.81667577	0.34904820	-1.98257023
H	-2.75417164	0.33064875	-2.30161961
O	-4.36378452	0.49175900	-2.44387212
O	-8.27520979	1.24901967	-0.29193384
O	-4.47219401	2.50368059	1.84733342
S	8.67452101	2.64214840	0.45113272

Supplementary Table 4. Cartesian coordinates of optimized *syn*-D2-D2 in Gaussian package.

C	4.36799326	-1.86006576	0.00946479
C	4.64611223	-2.02380320	1.36139417
H	3.86759120	-2.02540800	2.11633093
C	5.97554718	-2.15497873	1.74521479
H	6.21020570	-2.26747264	2.79939137
C	7.01641877	-2.12833986	0.80783144
C	6.71279777	-1.94538055	-0.54634413
H	7.49690409	-1.90967299	-1.29544482
C	5.38973299	-1.81008471	-0.93366200
C	4.81329632	-1.61761859	-2.31465836
H	5.08249372	-2.44520445	-2.97820068
H	5.16777503	-0.69286191	-2.77736355
C	3.28979977	-1.55614568	-2.07402564
H	2.85335724	-0.59766086	-2.36782150
H	2.75187557	-2.35637257	-2.59297013
C	9.69810650	-1.71551967	0.09467997
H	9.68264119	-2.36044350	-0.78779176
H	10.71575790	-1.69771542	0.49157203
H	9.39484005	-0.69545158	-0.15522311
C	1.91612924	-1.76012950	-0.03602510
H	1.93615405	-1.86974953	1.04516651
C	0.71224339	-1.67269301	-0.68787747
H	0.66423552	-1.54820854	-1.76335036
C	-0.49529778	-1.70010772	0.03303124
H	-0.45045879	-1.77529579	1.11658482
C	-1.75120230	-1.61851751	-0.54674896
C	-2.85328539	-1.59793877	0.32623845
H	-2.58051903	-1.64093293	1.37766014
C	-4.23125412	-1.50245461	0.15855381
C	-4.92802894	-1.51642608	-1.10438834
C	-7.06601289	-1.32479550	0.10352247
C	-4.98675659	-1.38397568	1.40885892
C	-7.06331515	-1.48285517	-2.32235044
H	-6.41031847	-1.08946491	-3.10013320
H	-7.92906199	-0.82980656	-2.21089745
C	-7.49514887	-2.90470648	-2.65755539
H	-8.14612092	-3.30120760	-1.87368211
H	-6.62114977	-3.55396319	-2.76318631
H	-8.04762050	-2.91533356	-3.60237831
C	-7.16321355	-1.15036950	2.52528982
H	-6.52464112	-0.63699980	3.24336801
H	-8.02189328	-0.51858932	2.29804669
C	-7.60073608	-2.50664445	3.06215661
H	-8.17791553	-2.37476249	3.98279756
H	-6.72940732	-3.12804783	3.28883433
H	-8.23169454	-3.02339928	2.33318933
N	3.11990407	-1.72528894	-0.62298331
N	-6.31241559	-1.41911601	-1.06326154
N	-6.37514464	-1.27692653	1.29419270
O	-1.81065691	-1.50600876	-1.89332829
H	-2.75601914	-1.60451440	-2.16664805
O	-4.38889397	-1.61557193	-2.21904177
O	-8.28529242	-1.28461494	0.05901083
O	-4.46820214	-1.36452864	2.51697601
S	8.66106774	-2.37201951	1.42704518
C	-4.36805436	1.85613299	0.08516107
C	-4.64707083	1.94856491	1.44366932
H	-3.86931314	1.90924793	2.19835726
C	-5.97675259	2.05967412	1.83290807
H	-6.21219106	2.11580371	2.89139998
C	-7.01692477	2.08306269	0.89468345
C	-6.71231235	1.97252968	-0.46710849
H	-7.49583928	1.97747782	-1.21767124
C	-5.38903961	1.85707422	-0.86010722
C	-4.81172813	1.73633510	-2.24883899
H	-5.16607726	0.83669204	-2.75864335
H	-5.08041564	2.59705524	-2.86901857
C	-3.28846351	1.66231006	-2.01074943
H	-2.75043275	2.48954468	-2.48538465
H	-2.85137317	0.72119872	-2.35492986
C	-9.69797320	1.70150289	0.16173959
H	-9.39361379	0.69473417	-0.13613704
H	-10.71578156	1.66364589	0.55679249
H	-9.68275481	2.38781384	-0.68893615
C	-1.91613101	1.75730977	0.03586168
H	-1.93648169	1.80947291	1.12132210
C	-0.71205881	1.70575862	-0.61944490
H	-0.66361168	1.63861371	-1.69996215
C	0.49519186	1.69746562	0.10228991
H	0.44990591	1.71567534	1.18826519
C	1.75137669	1.64805994	-0.48052963
C	2.85313258	1.58267442	0.39050322
H	2.57980513	1.57137847	1.44257076
C	4.23119458	1.49554119	0.21858750
C	4.92809929	1.57424367	-1.04178539
C	7.06567470	1.31495268	0.15433807
C	4.98643831	1.31348840	1.46133850
C	7.06294113	1.59601484	-2.26073065
H	7.92492054	0.93287124	-2.18596418
H	6.40718754	1.24839895	-3.05775623
C	7.50249273	3.03127086	-2.52033328
H	6.63201246	3.69001225	-2.59028267
H	8.15641622	3.38199751	-1.71735272
H	8.05406662	3.08899905	-3.46397491
C	7.16246434	1.02566200	2.56533666
H	8.02338878	0.40902255	2.30750753
H	6.52544304	0.47503260	3.25670286
C	7.59533768	2.35513998	3.16887314
H	8.17257613	2.17974540	4.08218654
H	8.22496060	2.90936042	2.46671648
H	6.72194285	2.96181647	3.42546151
N	-3.11964870	1.75293157	-0.55261097
N	6.31224822	1.46945367	-1.00619358
N	6.37475432	1.21085333	1.34142693
O	1.81107874	1.60544142	-1.83119800
H	2.75633537	1.71912197	-2.09898332
O	4.38926094	1.73378087	-2.14954652
O	8.28482055	1.27304742	0.10751898
O	4.46791548	1.23939763	2.56715867
S	-8.66211620	2.29424483	1.52457333

Supplementary Table 5. Cartesian coordinates of optimized *anti*-D3-D3 in Gaussian package.

C	-7.39524676	1.79169691	-0.82839197
C	-5.56105079	1.50932129	0.69073778
C	-4.72318942	1.34424785	-0.48085262
C	-5.35209039	0.98628131	-1.75843066
C	-8.83006558	1.31113905	-0.83154127
H	-9.26583225	1.46141962	-1.82219825
H	-9.40933273	1.87272274	-0.09430048
H	-8.85715527	0.24883145	-0.57615042
C	-7.25600266	3.27639828	-1.14663315
H	-7.66227183	3.47581271	-2.14127921
H	-6.20676186	3.58528740	-1.12925737
H	-7.80642458	3.86464181	-0.40826916
C	-3.33553228	1.36080550	-0.49205445
H	-2.93416916	1.23796358	-1.49430106
C	-2.33952640	1.48543922	0.49728522
C	-1.03310220	1.53784642	0.04124363
H	-0.88935713	1.44490635	-1.03162561
C	0.12017184	1.69694156	0.83467295
H	0.01887591	1.79429367	1.91002660
C	1.34304986	1.73579952	0.21020291
H	1.37679342	1.61675909	-0.86941059
C	2.75302831	2.05836138	2.22768075
H	2.55315544	1.09708321	2.71352684
H	2.06516326	2.80838014	2.62743675
C	4.23703530	2.45610445	2.37168053
H	4.34191169	3.51380802	2.63710516
H	4.72995205	1.85401761	3.13732934
C	4.80369527	2.18778347	0.99995508
C	3.77584636	1.89441203	0.10739840
C	6.11773266	2.16366610	0.57369187
H	6.92616516	2.34432385	1.27619597
C	6.40212410	1.87232788	-0.76882896
C	5.35538002	1.59711023	-1.65130981
H	5.56192838	1.34502466	-2.68469336
C	4.03086694	1.58817798	-1.22005425
H	3.24626718	1.29658731	-1.91015094
C	8.13048352	0.75936517	-2.67370435
H	9.18355333	0.54912961	-2.87550050
H	7.68925357	1.20703758	-3.56736454
H	7.61882870	-0.17204007	-2.42073775
N	2.53841641	1.91421181	0.78067431
S	8.10760152	1.90239313	-1.26494982
O	-6.89527862	1.53389512	0.48493132
O	-6.70846360	1.01560538	-1.79741168
O	-5.18745785	1.59713174	1.85384063
O	-4.75535171	0.61713991	-2.74877940
O	-2.54815391	1.53922272	1.83145143
H	-3.52032946	1.55978282	1.99750346
C	7.39527925	-1.79206937	0.82826056
C	5.56104264	-1.50941360	-0.69066625
C	4.72325346	-1.34413316	0.48093451
C	5.35229830	-0.98630242	1.75847376
C	8.83017887	-1.31178918	0.83146948
H	9.26599169	-1.46254409	1.82203588
H	9.40926103	-1.87323509	0.09397627
H	8.85749066	-0.24940910	0.57643965
C	7.25580559	-3.27682613	1.14620719
H	7.66205084	-3.47651097	2.14080844
H	6.20650770	-3.58552912	1.12879422
H	7.80610797	-3.86502084	0.40771615
C	3.33558774	-1.36029878	0.49214981
H	2.93426611	-1.23734881	1.49440169
C	2.33953177	-1.48467147	-0.49717892
C	1.03310209	-1.53686774	-0.04112729
H	0.88935375	-1.44385709	1.03173470
C	-0.12016850	-1.69593800	-0.83458370
H	-0.01881817	-1.79339197	-1.90992261
C	-1.34306588	-1.73480654	-0.21015785
H	-1.37686053	-1.61566179	0.86944021
C	-2.75294693	-2.05779388	-2.22764761
H	-2.55316762	-1.09655137	-2.71359947
H	-2.06495743	-2.80775135	-2.62731114
C	-4.23688788	-2.45580038	-2.37165294
H	-4.34158443	-3.51347454	-2.63725529
H	-4.72994213	-1.85364519	-3.13715172
C	-4.80357837	-2.18771234	-0.99990246
C	-3.77582752	-1.89393692	-0.10738692
C	-6.11762280	-2.16411723	-0.57360753
H	-6.92599101	-2.34516545	-1.27608574
C	-6.40210992	-1.87288314	0.76890381
C	-5.35544754	-1.59709256	1.65131248
H	-5.56203135	-1.34496845	2.68466866
C	-4.03094865	-1.58766699	1.22003897
H	-3.24645551	-1.29567886	1.91009138
C	-8.13128839	-0.75980294	2.67293791
H	-9.18462709	-0.55241174	2.87626568
H	-7.68735467	-1.20528601	3.56633176
H	-7.62272456	0.17270810	2.41790014
N	-2.53839046	-1.91345716	-0.78065486
S	-8.10753675	-1.90417643	1.26524724
O	6.89527031	-1.53391625	-0.48497300
O	6.70865018	-1.01609142	1.79747815
O	5.18733801	-1.59738093	-1.85373448
O	4.75570136	-0.61693492	2.74882431
O	2.54812023	-1.53844977	-1.83135013
H	3.52028804	-1.55937862	-1.99742380

Supplementary Table 6 Cartesian coordinates of optimized *syn*-D3-D3 in Gaussian package.

C	7.22986723	-2.16770701	-0.04516421
C	5.24631666	-1.38365160	-1.11696234
C	4.60488963	-1.46396951	0.18240173
C	5.45266608	-1.44197818	1.38275197
C	6.95414048	-3.66764327	-0.06546781
H	7.47187078	-4.14402865	0.77070052
H	7.31665378	-4.09552244	-1.00342864
H	5.88371852	-3.87366689	0.02384481
C	8.69972107	-1.83217393	-0.17248305
H	9.25155695	-2.28254012	0.65643303
H	8.82910919	-0.74748522	-0.14230462
H	9.08758217	-2.22208691	-1.11672753
C	3.23576023	-1.42948106	0.41765210
H	2.99842756	-1.43494121	1.47860066
C	2.10272250	-1.41527291	-0.41942075
C	0.85675763	-1.47691145	0.18400350
H	0.82381420	-1.51908498	1.26995461
C	-0.35142344	-1.50955001	-0.53638235
H	-0.29610974	-1.44332991	-1.61657512
C	-1.56413240	-1.60559721	0.09833704
H	-1.60698266	-1.64275294	1.18400997
C	-2.88995618	-1.67124836	-1.98337837
H	-2.24986112	-2.45328324	-2.40349148
H	-2.55347781	-0.70301698	-2.36526869
C	-4.38938060	-1.92427435	-2.24895086
H	-4.81535748	-1.14006925	-2.87887696
H	-4.55046856	-2.88841851	-2.74257168
C	-5.00168424	-1.90558654	-0.87160144
C	-4.01442085	-1.75379129	0.09457355
C	-6.33431157	-2.00023340	-0.50561501
H	-7.08879911	-2.10535517	-1.27708479
C	-6.67695178	-1.94830530	0.84920121
C	-5.67108267	-1.77228252	1.80796230
H	-5.93634605	-1.68832574	2.85711003
C	-4.33411599	-1.67179275	1.44426862
H	-3.58586089	-1.49425862	2.20883581
C	-9.30079774	-2.38712322	-0.04077002
H	-10.33493322	-2.51378115	0.28732126
H	-8.97983015	-3.29995588	-0.54941568
H	-9.25434328	-1.53896209	-0.73014517
N	-2.75077716	-1.67250474	-0.51814108
S	-8.33820786	-2.08844499	1.46060771
O	6.58262731	-1.54145036	-1.15313587
O	6.79016528	-1.60201948	1.17914213
O	4.69565698	-1.13977051	-2.18662997
O	5.06659617	-1.25111019	2.51388323
O	2.12827809	-1.38270371	-1.77218228
H	3.06628277	-1.30676342	-2.06861372
C	-7.18519557	2.07375785	0.32308541
C	-5.27097624	1.42358879	-0.94432095

C	-4.50955518	1.60230081	0.27683688
C	-5.22049529	1.54171313	1.56522233
C	-8.62938982	1.62411994	0.36304736
H	-9.13365234	2.08132035	1.21760211
H	-9.13608312	1.92156876	-0.55834968
H	-8.66610958	0.53863178	0.47664585
C	-7.03756194	3.58959412	0.23519193
H	-7.49555305	4.05011849	1.11393738
H	-5.98482821	3.88324363	0.19685373
H	-7.53696884	3.95687839	-0.66491370
C	-3.12859027	1.69209803	0.36596833
H	-2.78868441	1.74435463	1.39720584
C	-2.08268151	1.73978306	-0.57752922
C	-0.79757990	1.84460602	-0.07781484
H	-0.69422478	1.90069605	1.00296321
C	0.37773571	1.87420308	-0.85341027
H	0.29675360	1.80512800	-1.93205324
C	1.59577711	1.93782818	-0.22793378
H	1.62939898	1.98166975	0.85745181
C	2.97607187	1.87179199	-2.27960773
H	2.56951937	0.91706074	-2.62586483
H	2.41904804	2.68291408	-2.75850893
C	4.50091101	1.98017272	-2.50226634
H	4.76462268	2.91843880	-3.00152267
H	4.87045825	1.15183954	-3.11046465
C	5.06908599	1.93152869	-1.10578094
C	4.03882312	1.93119059	-0.16826783
C	6.38462834	1.85753178	-0.68900634
H	7.18916741	1.81425142	-1.41754075
C	6.67374174	1.81288347	0.68304073
C	5.62793578	1.82836489	1.60772918
H	5.83335291	1.77200594	2.67006870
C	4.29960857	1.87436035	1.19222951
H	3.50940518	1.84116073	1.93450500
C	8.33581614	0.94210509	2.76462464
H	9.36937011	0.67677934	2.99986525
H	7.95826093	1.59695381	3.55348436
H	7.73423586	0.03236198	2.70194998
N	2.79477887	1.95267726	-0.82289029
S	8.38578693	1.78246756	1.15719757
O	-6.61282095	1.46410659	-0.83768946
O	-6.57824990	1.58152122	1.50459930
O	-4.81218151	1.19296755	-2.05936805
O	-4.69203596	1.41770585	2.64635726
O	-2.23133307	1.68630338	-1.92281317
H	-3.18319256	1.53058951	-2.12655416

Supplementary Table 7 Cartesian coordinates of optimized *syn*-D1-D3 in Gaussian package.

C	-4.34375828	-1.97362632	-0.97952176
C	-5.28071366	-1.57769671	-1.93704706
C	-6.63277559	-1.72732813	-1.68721370
H	-7.36610069	-1.41535018	-2.42607972
C	-7.04846405	-2.27836568	-0.47266773
H	-8.10689100	-2.37996329	-0.25763499
C	-6.10466637	-2.67149002	0.47025940
H	-6.43378287	-3.08771420	1.41740989
C	-4.73718836	-2.52048438	0.23584118
H	-4.01662427	-2.81974916	0.99022070
C	-3.09161410	-0.97864213	-2.70792088
H	-2.40058479	-1.43358398	-3.42346242
H	-2.76197007	0.05291118	-2.52997181
C	-4.56407765	-1.06136267	-3.16170141
H	-4.93872582	-0.09048210	-3.49909633
H	-4.67854017	-1.75802262	-3.99951836
C	-1.88765134	-1.98399336	-0.80011101
H	-1.99023591	-2.58768219	0.09805892
C	-0.65924593	-1.56307642	-1.20969728
H	-0.55289014	-0.92112144	-2.07718392
C	0.52453656	-1.88415616	-0.49811899
H	0.46068299	-2.52123687	0.37942420
C	1.76226006	-1.39751964	-0.86183696
C	2.85918420	-1.76466693	-0.03867648
H	2.58383547	-2.39838385	0.79987551
C	4.20684891	-1.45952302	-0.03423204
C	4.89941909	-0.66441314	-1.02073278
C	6.99116511	-0.89882239	0.25931729
C	4.95722837	-2.00535769	1.09765197
C	6.91877742	0.35193465	-1.88860835
H	7.76762371	0.86563935	-1.44397937
H	6.19174302	1.08819272	-2.22755900
C	7.37290247	-0.54540554	-3.03116952
H	6.52000728	-1.05882478	-3.48309973
H	8.09616357	-1.28514883	-2.67563836
H	7.85522387	0.06203010	-3.80334554
C	6.99558422	-2.11179167	2.41315954
H	6.24299643	-2.12887381	3.20035700
H	7.76599401	-1.38603469	2.66643671
C	7.58887738	-3.49903406	2.20821608
H	8.33081875	-3.48989893	1.40497074
H	6.80135590	-4.21862648	1.96881474
H	8.08401059	-3.82481457	3.12852487
N	-3.04772398	-1.71742416	-1.44414507
N	6.25795230	-0.41886456	-0.81487098
N	6.30603218	-1.61646184	1.20780222
O	1.81934286	-0.58663759	-1.93246437
H	2.76211255	-0.35101253	-2.11053161
O	4.37984124	-0.21070785	-2.04522780
O	4.47775311	-2.75828446	1.92703665
S	8.63640549	-0.61987252	0.38431510
C	5.07303038	2.74428414	0.97226720
C	3.28144045	2.33525732	-0.54961383
C	2.62541927	1.65325975	0.56706046
C	3.46173893	1.14333397	1.67530922
C	6.58029787	2.81009162	0.87412452
H	7.01002419	2.89501127	1.87481179
H	6.87361542	3.67842364	0.27953113
H	6.96932925	1.90513684	0.40759745
C	4.48585406	3.96133074	1.68197109
H	4.88370384	4.01409336	2.69829132
H	3.39506201	3.90926843	1.73732402
H	4.76446359	4.86858982	1.14022524
C	1.28320433	1.37069577	0.66828418
H	1.04312506	0.81276934	1.56945778
C	0.14446772	1.67946875	-0.13190669
C	-1.07663893	1.31606069	0.37788922
H	-1.08892452	0.77900426	1.32192038
C	-2.32626106	1.61271918	-0.24017821
H	-2.31222090	2.20599459	-1.14880949
C	-3.49473021	1.18016530	0.30583972
H	-3.47471330	0.59003091	1.21835183
C	-4.98941431	2.14186371	-1.42317032
H	-4.35380631	1.76073977	-2.22813588
H	-4.73394489	3.19811071	-1.26984646
C	-6.49453639	1.94336503	-1.70344704
H	-6.98151689	2.88205321	-1.98019470
H	-6.65312965	1.23455373	-2.52429630
C	-7.01785977	1.37027605	-0.40947455
C	-5.94654022	1.05270410	0.42733759
C	-8.31348338	1.10866061	-0.01923963
H	-9.14464505	1.35255576	-0.67611181
C	-8.55368434	0.51969333	1.23331142
C	-7.47583040	0.22686703	2.06772873
H	-7.63695096	-0.21871626	3.04274101
C	-6.16274749	0.49539022	1.67656321
H	-5.34570761	0.25677625	2.34894072
C	-10.16659628	-0.43392186	3.32667793
H	-11.19890927	-0.62147984	3.63003322
H	-9.73232480	0.30971244	4.00001313
H	-9.60806789	-1.37154323	3.39099203
N	-4.73641259	1.39312825	-0.19226646
S	-10.25236390	0.18092684	1.62856911
O	4.57762076	2.66926872	-0.36667046
O	4.76027702	1.55132658	1.67675626
O	2.78400383	2.58945906	-1.63237610
O	3.08934485	0.37655762	2.53045651
O	0.17817553	2.33022171	-1.30912736
H	1.11228948	2.39705868	-1.61382299

Supplementary Table 8 Cartesian coordinates of optimized *anti*-D1-D3 in Gaussian package.

C	4.60603529	-2.43350626	-0.43928749
C	5.77606455	-1.97061204	-1.04366335
C	6.99128682	-2.56309139	-0.74978889
H	7.90250417	-2.19747587	-1.21482808
C	7.03166723	-3.62749221	0.15493128
H	7.97847804	-4.10115373	0.39333027
C	5.85730067	-4.08061481	0.75270084
H	5.89448347	-4.90593331	1.45709968
C	4.62618756	-3.48768864	0.46857878
H	3.72353132	-3.84427855	0.95420235
C	3.94792885	-0.58715319	-1.75249094
H	3.75286254	0.37652544	-1.26892875
H	3.36941986	-0.62159930	-2.68124165
C	5.45653072	-0.83081983	-1.97722996
H	5.66184762	-1.10807355	-3.01658205
H	6.04718688	0.06067956	-1.75050335
C	2.20470256	-1.92725843	-0.60660247
H	2.02172723	-2.83147917	-0.03216209
C	1.15819019	-1.15788130	-1.01446128
H	1.32375140	-0.22937572	-1.54939167
C	-0.18584016	-1.53037325	-0.75448937
H	-0.38177514	-2.46369006	-0.23517291
C	-1.26409538	-0.75869233	-1.13158362
C	-2.55295256	-1.29295348	-0.87441121
H	-2.53715833	-2.24850357	-0.35689563
C	-3.84154043	-0.84799641	-1.10842300
C	-4.20456970	0.37194320	-1.79447746
C	-6.57726532	-0.05897811	-1.31191701
C	-4.89909519	-1.72463542	-0.60715442
C	-5.84027773	2.08603830	-2.31528100
H	-4.98426537	2.70689765	-2.05554366
H	-6.71497353	2.45894028	-1.78696796
C	-6.07059667	2.05965067	-3.81934420
H	-6.92612558	1.42661516	-4.07096121
H	-5.18130645	1.69259137	-4.33858456
H	-6.28013668	3.07437726	-4.17264814
C	-7.25227291	-2.18799431	-0.23928951
H	-8.10270510	-1.59599099	0.09293590
H	-6.81148917	-2.70278453	0.61329880
C	-7.67040401	-3.18111343	-1.31492738
H	-6.81350369	-3.77906346	-1.63714266
H	-8.09552977	-2.65983643	-2.17744702
H	-8.43084029	-3.85882680	-0.91430893
N	3.50961161	-1.67561391	-0.87086986
N	-5.54929655	0.74497233	-1.76697875
N	-6.22120655	-1.25391154	-0.72694067
O	-1.00974764	0.43720185	-1.69617035
H	-1.85849360	0.81189296	-2.04022337
O	-3.41134379	1.10127110	-2.39529144
O	-4.69132501	-2.82003009	-0.11309901
S	-8.17833453	0.39560568	-1.47603129
C	-5.58870512	1.05572778	2.43295787
C	-3.53464376	-0.13838655	2.20237254
C	-3.00733086	1.07674603	1.57896672
C	-3.97044720	2.02537937	0.97730653
C	-7.05149703	0.68665014	2.33475122
H	-7.66013030	1.59346827	2.32425917
H	-7.33365990	0.06800344	3.18991818
H	-7.23470635	0.13510180	1.41223798
C	-5.26431593	1.84340998	3.69825084
H	-5.84287773	2.77031405	3.70531313
H	-4.20153450	2.09576563	3.75263073
H	-5.52768373	1.24919491	4.57669465
C	-1.67898931	1.36740290	1.37337535
H	-1.52989806	2.26766528	0.78351321
C	-0.46509965	0.74075144	1.78164428
C	0.70720396	1.34153509	1.39958142
H	0.64737391	2.24545302	0.80094729
C	1.98927745	0.81975407	1.73482880
H	2.01471542	-0.06723583	2.35792809
C	3.13469831	1.36795745	1.25472547
H	3.09165170	2.24531733	0.61444506
C	4.63040652	-0.28725744	2.32356953
H	4.05573569	-1.13202199	1.92693562
H	4.28766730	-0.09682648	3.34566705
C	6.15123704	-0.53772535	2.23427225
H	6.64065578	-0.36003576	3.19743765
H	6.37007300	-1.56619377	1.93438377
C	6.61601792	0.45905152	1.20278925
C	5.55313403	1.28643922	0.83046511
C	7.85790977	0.61556056	0.62678592
H	8.67518746	-0.04422553	0.90656554
C	8.05954355	1.62195864	-0.33396964
C	6.99683736	2.45717936	-0.67891277
H	7.12873765	3.24622125	-1.41046244
C	5.73304176	2.29741411	-0.10219872
H	4.92419064	2.95664191	-0.40028348
C	9.54685722	3.08042802	-2.21808215
H	10.52962939	3.17447621	-2.68514271
H	9.30421897	4.02356324	-1.72154919
H	8.80921546	2.86276796	-2.99511065
N	4.38630899	0.89782292	1.49628206
S	9.68900365	1.72181900	-1.03385748
O	-4.86218009	-0.17577881	2.42193330
O	-5.28001099	1.81869816	1.27614143
O	-2.89459545	-1.13950358	2.48104183
O	-3.67975953	2.92073836	0.22056287
O	-0.39012388	-0.37779289	2.53091023
H	-1.27471080	-0.81050772	2.55266911

9. Reference

1. Berraud-Pache, R. et al. Redesigning donor-acceptor Stenhouse adduct photoswitches through a joint experimental and computational study. *Chem. Sci.* 12, 2916–2924 (2021).
2. Duan, Y. et al. Controlling isomerization of photoswitches to modulate 2D logic-in-memory devices by organic-inorganic interfacial strategy. *Adv. Sci.* 10, 2207443 (2023).
3. Helmy, S. et al. Photoswitching using visible light: A new class of organic photochromic molecules. *J. Am. Chem. Soc.* 136, 8169–8172 (2014).
4. Adak, O. et al. Flicker noise as a probe of electronic interaction at metal-single molecule interfaces. *Nano Lett.* 15, 4143–4149 (2015).
5. Tang, C. et al. Multicenter-bond-based quantum interference in charge transport through single-molecule carborane junctions. *Angew. Chem. Int. Ed.* 58, 10601–10605 (2019).
6. Wang, H. et al. Gating the rectifying direction of tunneling current through single-molecule junctions. *J. Am. Chem. Soc.* 146, 35347–35355 (2024).
7. Li, D. et al. Wavelet transform-based clustering decoding the dynamical properties of single molecular junctions. *J. Phys. Chem. Lett.* 17, 2601–2609 (2026).
8. Lu, T. & Chen, F. Multiwfn: a multifunctional wavefunction analyzer. *J. Comput. Chem.* 33, 580–592 (2012).
9. Lu, T. Visualization analysis of covalent and noncovalent interactions in real space. *Angew. Chem. Int. Ed.* 64, e202504895 (2025).